PHOTOSENSITIVE SELENIUM NANOPARTICLES TETHERED TO SILICON NANOWIRES FOR SOLAR ENERGY CONVERSION

A Project Report Submitted

as part of the requirements for the degree of

MASTER OF SCIENCE

Submitted By

DEBANJAN MAITY

Roll No. CY17MSCST11005

Under the supervision of

Dr. M. DEEPA

to the

DEPARTMENT OF CHEMISTRY

INDIAN INSTITUTE OF TECHNOLOGY HYDERABAD

INDIA

MAY, 2019

Declaration

I hereby declare that the matter embodied in this report is the result of investigation carried out by me in the Department of Chemistry, Indian Institute of Technology Hyderabad under the supervision of **Dr. M. Deepa**

In keeping with general practice of reporting scientific observations, due acknowledgement has been made wherever the work described is based on the findings of other investigators.

9/5/2019

Signature of the Supervisor

Dr. M. Deepa
Head & Professor
Department of Chemistry
Indian Institute of Technology Hyderabad
Kandi-502285, Sangareddy, Telangana, India

Debanjan Maity.

(Signature)

Debanjan Maity.

(Student Name)

CY17MSCST11005

(Roll No)

Approval Sheet

This thesis entitled "**Photosensitive selenium nanoparticles tethered to silicon nanowires for solar energy conversion**" by Debanjan Maity is appproved for the degree of Master of Science from Indian Institute of Technology Hyderabad.

Name and affiliation

Examiner

Name and affiliation

Examiner

9/5/2019

Name and affiliation

Dr. M. Deepa
Head & Supervisor Professor
Department of Chemistry
Indian Institute of Technology Hyderabad
Kandi-502285, Sangareddy, Telangana, India

Acknowledgements

I would like to express my deep sense of gratitude to my supervisor, **Dr. M. Deepa**. It has been a huge learning experience for me to be working under her exemplary guidance. Her motivation and care kept me moving in pursuit of my goal. Her advice and encouragement were immensely helpful for the successful completion of this project and organizing my thesis.

I would like to specially thank my senior, **Ms. Ankita Kolay** for her constant support and motivation. She helped me learning new concepts and guided me during difficult times. Her invaluable inputs and deep insight were instrumental for the completion of this project. Also I would like to thank my seniors, Ms. Aparajita Das, Mr. Manoranjan Ojha, Mr. Sathish Deshagani for their encouragement and cooperation during research project.

I am grateful to our head of the department, Dr. M. Deepa and to the entire Department of Chemistry, IIT Hyderabad for providing me the opportunity to do research.

Finally, I would like to thank my beloved parents and friends for their constant moral boost.

Abstract

This work aims at fabricating different types of liquid junction silicon nanowire solar cells and testing their photovoltaic performance. Se NPs are p-type, visible light responsive electrically conductive material that has been synthesized using a very simple and facile hydrothermal method. The n-type silicon wafers are etched using metal catalyzed electroless etching method to produce SiNWs. The SiNWs because of its several beneficial optical and structural properties is applied as photoanode. 0.05 M Br_2 in 8.6 M HBr redox mix is used as electrolyte and carbon fabric as counter electrode. The highly expensive Pt electrode which is reported in previous literature is replaced with robust and highly conductive carbon cloth which reduces the cost of device fabrication. When SiNWs is used as photoanode the solar cell gives an efficiency of 4.91%. But when this SiNWs are modified by dropcasting photoconductive SeNPs over it then 43% rise in efficiency is observed. This rise in efficiency is mainly attributed to the hole transporting property of Se NPs through its c axis of hexagonal crystal structure. This facile hole transportation reduces charge recombination in electrode-electrolyte interface and enhances solar cell performance. The previously reported electrocatalytic metal NPs like Au and Pt are replaced by Se. The expensive Metal nanoparticles like Au and Pt can only act as electron trappers where as SeNPs are hole conductors and thus can rapidly transport the photogenerated holes. These photogenerated holes causes photooxidation and reduces the device performance and stability. But in presence of hole transporting material like Se NPs photooxidation is minimized and device performance is further improved compare to Au nanoparticle decorated SiNWs electrode. To prove this statement a control cell experiment is performed. The results show a 1.5 times rise in efficiency when SiNWs are decorated using Se NPs but for Au NPs the efficiency is almost same as the pristine SiNWs electrode. Optical, structural, PEC, and impedance studies furnish a deep understanding of the phenomena involved in yielding a superior performing liquid-junction PEC solar cell based on the Se NPs@Si NW photoanode.

Contents

List of Figures

List of tables

1. Introduction……....**1**

1.1 P-N junction solar cells……**2**

1.1.1 Working principle…….. **2**

1.2 Silicon nanowire solar cells…….... **3**

1.2.1 P-N junction silicon nanowire solar cells……...**4**

1.2.2 Liquid junction silicon nanowire solar cells……...**4**

1.3 Literature survey……..**4**

1.3.1 Silicon nanowire array photoelectrochemical solar cells……...**4**

1.3.2 Double-walled carbon nanotubes used as counter Electrode ……**5**

1.3.3 Platinum nanoparticle for solar energy conversion……**6**

1.3.4 SiNW cell with passivated & modified surface……**6**

1.3.5 Ionic liquid electrolyte based SiNW solar cells……**7**

1.3.6 Aqueous ferrocyanide/ferricyanide redox electrolyte based SiNW cells…...**8**

2. Objectives of This Work…….**10**

3.Experimental……**10**

3.1 Chemicals…….....**10**

3.2 Preparation of trigonal Se……...**10**

3.3 Etching of silicon wafer……..**11**

3.4 Photovoltaic device fabrication……...**11**

4. Results and discussion…….**12**

4.1 Structural characterization……...**12**

4.1.1 SEM analysis……**12**

4.1.2 TEM analysis……**13**

4.1.3 Raman analysis……..**14**

4.1.4 XRD analysis……**14**

4.1.5 AFM analysis……**15**

4.2 Optical characterization……**16**

4.2.1 Absorption spectral analysis……..**16**

4.2.2 Diffuse reflectivity spectral analysis……**17**

4.3 Photoelectrochemical characterization……..**18**

4.3.1 Photoconductivity measurement……...**18**

4.3.2 Mott-schottky plot……**.....18**

4.3.3 Cyclic voltammetry……...**19**

4.3.4 Energy profile diagram ……**20**

4.3.5 Solar cell characterization ……**21**

4.3.6 IPCE Measurement ……...**22**

4.3.7 Impedance studies……..**24**

4.3.8 Transient photovoltage analysis……**25**

4.3.9 Transient photocurrent analysis……**26**

4.3.10 Solar cell stability……**27**

4.3.11 Control cell experiment……....**28**

5. Alternate HTL and CE……...**30**

5.1 Photoanode……**30**

5.1.1 Synthesis of PEDOT/SiNWs……...**30**

5.2 Counter electrode……...**30**

5.2.1 Synthesis of WO_3/FTO……**30**

5.3 Electrolyte……**31**

6. Conclusion……**32**

References

List of Figure

1.1 A traditional p-n junction……**2**

1.1.1 Working of a solar cell……**3**

1.3.1 Schematic presentation of the PEC based on n-SiNW array……...**5**

1.3.2 PEC composed of SiNW arrays, the DWNT film and redox electrolyte…….**5**

1.3.3 Graphical presentation of PtNP-decorated n-SiNW arrays prepared by aqueous electroles etching of silicon followed by electroless metal deposition…….....**6**

1.3.4 Schematic illustration of the fabrication process of a PtNPs@C@SiNW array. a) SiNW array prepared by the MCEE method. b) C/Si core/shell nanowire array after carbon MPECVD. c) PtNPs@C@SiNW array after PtNP EMD……....**7**

1.3.5 Graphical presentation of the PEC cell structure using SiNWs as electrode. The vertical SiNWs surface is anchored by methyl groups and decorated with Pt nanodots. The space between SiNWs is filled with electrolyte. Light passes through the top transparent ITO-coated glass electrode……...**8**

3.3 Schematic presentation of vertically aligned silicon NWs after anisotropic etching.....**11**

3.4(a) Illustration of Fabrication of Si NWs, Se NPs@Si NWs, and Se NPs@ n-Si Photoanodes through Photographs…….....**11**

3.4(b) Schematic of the Preparation of Se NPs@Si NWs and the Liquid-Junction PEC Solar Cell…….....**12**

4.1.1 SEM image of **(a)** SiNWs; inset shows the image of an n-Si wafer **(b)** Cross sectional view **(c)** top view of SiNWs **(d)** dense network of SiNWs **(e-f)** SeNPs@SiNWs**(g)** top view of SeNPs@SiNWs **(h)** C fabric…….....**13**

4.1.2 (a) TEM image of Se NPs; inset shows the SAED pattern **(b)** HRTEM of SeNPs@SiNWs..... **14**

4.1.3 Raman Spectra of SeNPs@SiNWs and SiNWs…….....**14**

4.1.4 XRD patterns of **(a)** Se NPs **(b)** SeNPs@SiNWS; inset is an enlarged view of low 2θ region……....**15**

4.1.5 AFM topography images and section profiles of (a, a′) SiNWs (b, b′) SeNPs@SiNWs.**16**

4.2.1 Absorbance spectra of SeNPs, SiNWs and SeNPs@SiNWs.....**17**

4.2.2 Variation of reflectivity of n-Si, SiNWs, SeNPs@SiNWs with wavelength…….**17**

4.3.1 J-V plots of SeNPs recorded under 1 sun illumination……..**18**

4.3.2 Mott-Schottky plot of Se NPs recorded in dark…….**19**

4.3.3 Cyclic voltammetry of **(a)** SeNPs **(b)** SiNWs……**20**

4.3.4 Energy level diagram of the SeNPs@SiNWs-Br^-/Br_2-C fabric solar cell showing all possible modes of electron transfer under 1 sun illumination…….**21**

4.3.5 J-V characteristics of liquid junction PEC solar cells with different photoanodes, C fabric as the CE, and Br^-/Br_2 as the electrolyte under 1 sun irradiance (AM 1.5)…….**22**

4.3.6 IPCE vs wavelength curves for the solar cells with Se NPs@Si NWs and Si NWs photoanodes…….**23**

4.3.7 Nyquist plots of (a, b) solar cells with photoanode- Br^-/Br_2-C fabric with varying photoanodes in dark, over a frequency range of 10^6 to 0.1 Hz at V_{OC} and (c) solar cell with the SeNPs@SiNWs as photoanode under dark and under irradiance (50 $mwcm^{-2}$) at V_{OC}……..**24**

4.3.8 transient photovoltage decay plot of SeNPs@SiNWs and SiNWs……**26**

4.3.9 transient photocurrent decay plot of SeNPs@SiNWs and SiNWs…….**27**

4.3.10 Effect of 1 sun exposure (100 $mwcm^{-2}$) on cell parameters: V_{OC}, J_{sc}, FF, and PCE of SeNPs@SiNWs/Br^-/Br_3^-/C fabric solar cell on continuous illumination for 6h…….**28**

4.3.11 Absorption spectra of Au NPs. (b) J-V curves of the cells with Au NPs@Si NWs and Se NPs@Si NWs photoanodes under 100 mW cm^{-2} and (c) Nyquist plots of the same cells with photoanode-Br^-/Br_2-C-fabric configurations in dark, over a frequency range of 10^6 to 0.1 Hz at V_{OC}……...**29**

List of Tables

1.3 Solar cell parameters of liquid junction Si NWs based solar cells reported in literature...**8**

3.3.4 Energy level positions of the photoanode components……...**20**

3.5 Solar cell parameters of cells with 8.6 M HBr/0.05 M Br_2 aqueous solution electrolyte and C-fabric counter electrode under 1 sun illumination (100 mW cm^{-2}) are listed with the photoanodes (exposed cell area ~0.5 cm^2)……..**21**

4.3.7 EIS parameters obtained from the fitted Nyquist plots of liquid junction PEC solar cells with different photoanodes……...**25**

4.3.10 Effect of prolonged continuous 1 sun illumination on a cell with Se NPs@Si NWs/Br^-/Br_3^-/C-fabric configuration (active area ~0.5 cm^2)…….....**27**

4.3.11 Comparison between the solar cell parameters of Au NPs@Si NWs/Br^-/Br_3^-/C-fabric control cell, Se NPs@Si NWs photoanode and Si NWs based cell (active area 0.5 cm^2)…...**29**

5.1 Solar cell parameters of PEDOT@SiNWs/Br^-/Br_2/C fabric cell under 1sun illumination……..**30**

5.2 Solar cell parameters of SeNPs@SiNWs/Br^-/Br_2/CE cell under 1sun illumination with different CEs……**31**

5.3 Solar cell parameters of SiNWs/C fabric solar cell in different redox electrolyte under 1sun illumination…….**31**

1. INTRODUCTION

In 21st century the biggest challenges that mankind is facing are pollution and clean energy crisis. The burning of carbon based fossil fuels results in enormous pollution which is causing severe damage to human health and making earth difficult to live in. The one possible way to address this is to reduce the use of carbon based fossil fuels burning and increase the use of renewable energy sources (air, water, solar) instead. In recent times, solar energy is one among the most popular choice of all renewable energy sources. Photovoltaic technology converts solar energy to electricity. The fundamental of photovoltaic device is based on photoelectric effect. This effect was first observed by Edmond Becquerel in 1839.This effect states that light sensitive materials after absorbing photons, emits electrons. The physical explanation of this effect was later given by Einstein for which he was awarded with the Nobel prize in 1905.The first photovoltaic module was built by Gerald Pearson, Calvin Fuller, and Daryl Chaplin of Bell Laboratories in 1954, where it was found that silicon gave an electric charge when exposed to sunlight. Currently, 90% of commercial photovoltaic devices manufactured are made of solar-grade Si owing to its high natural abundance, mature processing technology, and excellent reliability in solar cells.[1]But commercialization of Si based photovoltaics is hindered because of its high production cost owing to the high purity requirement of Si wafer for solar cell applications.[2] As a replacement of highly expensive metal grade Si wafer in recent years Si nanowires have gained immense interest. Silicon is also a leading material that is used in photovoltaics industry. Si nanowires have attracted intense research.[3] These 1D semiconductor nanowires possess some attractive optical and structural properties which makes them useful for solar cell applications.[4] Silicon nanowire based solar cells are less sensitive to impurities, hence production cost of the solar cells can be lowered by a great extent. Therefore, it has huge potential to be commercialized.[5] The liquid electrolyte based Si nanowire solar cells offer cost advantages over its solid state counterpart but photocorrision and photooxidation are the two crucial factors which limit efficiency when a liquid electrolyte is in contact with the electrodes.[10] There are only very few reports on liquid junction silicon solar cells. Thus this topic offers many opportunities to explore further.

1.1 p-n Junction Silicon Solar Cell

A p-type material has holes as majority carriers and a n-type material has electrons as majority carriers. When a p-type material and a n-type material are joined, there is a concentration gradient. As a result of which the holes diffuse from p-type material to the n-type material exposing negative charge and electrons diffuse from the n-type material to the p-type material exposing positive charge causing the formation of depletion region between the two layers resulting in an electrical field across the junction. The resulting electrical field gives rise to voltage.

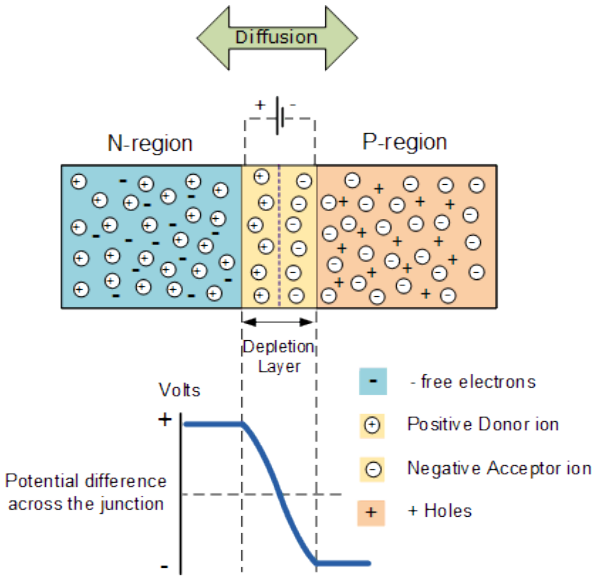

Figure 1.1: A traditional p-n junction.

1.1.1 Working Principle

A solar cell essentially consists of a silicon p-n junction diode with a glass window on the top surface of the p-type material which is made extremely thin so as to allow the incident photons to reach the junction easily. When light falls over the glass window of the solar cell, a current is produced which is known as light generated current and voltage across the terminals.

The formation of "light generated current" involves two key processes.

In the first process the photon striking on the transparent surface of the solar cell results in formation of electron-hole pair. This is only possible only if the photon striking on the glass wall of solar cell possesses higher energy compare to the band gap of semiconductor. But the generated electrons and holes are metastable species and they exist for a very short span of time before they recombine.

The second process involves the separation of the electron hole pair. The electric field generated in junction takes part and the minority charge carriers are swept across the p-n junction, where it becomes the majority carrier. Now if the emitter and the base of the solar cell are connected then current flows through the external circuit.

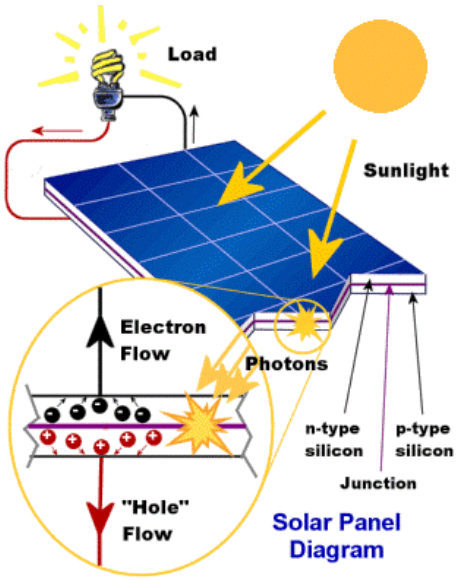

Figure 1.1.1: Working of a solar cell.

1.2 Silicon Nanowire Solar Cells

Silicon nanowire solar cells are the one in which one of the electrode in the solar cell is silicon nanowire.

There are lots of benefits of using silicon nanowire as semiconductor electrode.[6] These are:

- ✓ Increased surface area compared to planar electrode leads to greater absorption of sunlight.
- ✓ 1D nanostructure facilitates radial junction charge transport.
- ✓ Optical anti reflectivity over a wide range of solar spectrum.
- ✓ Rough surface of silicon nanowire leads to light scattering.
- ✓ Absorbs over a wide range of the electromagnetic spectrum from 300 nm to 1100 nm.
- ✓ Fabrication of silicon nanowire solar cells requires very low cost.
- ✓ Silicon nanowires are less sensitive to impurities compared to planar silicon electrodes.

Silicon nanowire solar cells can be classified into two types based on their fabrication. They are,

- p-n junction silicon solar cells.
- Liquid junction solar cells.

1.2.1 p-n Junction Silicon Nanowire Solar Cells

In a p-n junction silicon nanowire solar cell, a silicon nanowire electrode is used instead of using planar silicon electrode as in a p-n junction silicon solar cells.

A simple fabrication of silicon nanowire p-n junction solar cells consists of wafer scale arrays of n type silicon nanowires produced via solution phase etching method and deposition of p type amorphous Si using low pressure chemical vapour deposition method (LPCVD) and followed by thermal annealing.[7]

1.2.2 Liquid Junction Silicon Nanowire Solar Cells

In liquid junction Si nanowire solar cells, the photoanode or the photocathode is separated from the counter electrode by a liquid electrolyte containing redox active species. Under illumination, electronic excitation takes place in the semiconductor photo-active electrode generating electron-hole pair. The electron via external circuit reaches the counter electrode where it reduces the oxidized redox species and the reduced redox species accepts the hole from photo- active electrode. Liquid junction silicon solar cells have few advantages compared to solid state devices[8]. These are-

- The processing required to form a diffused junction in a solid state device is replaced by the simple immersion of the semiconductor in an electrolyte.
- The redox electrolytes which separates the anode and the cathode regenerates the photoactive component of the electrode.
- The redox electrolyte facilitates interfacial charge transfer and maintains ionic conduction between two electrodes.
- The use of a liquid junction provides a high quality, conformal and rectifying contact to the electrodes.

1.3 Literature Survey

1.3.1 Silicon Nanowire Array Photoelectrochemical Solar Cells[6]

In the year 2008 a study by Peng et al., reported a photoelectrochemical solar cell having silicon nanowire as photoanode and platinum mesh as a counter electrode in the presence of HBr/Br_2 electrolyte and showed a power conversion efficiency = 0.29% under 1 sun illumination. They used metal assisted electroless etching method to produce vertically aligned silicon nanowires for device fabrication.

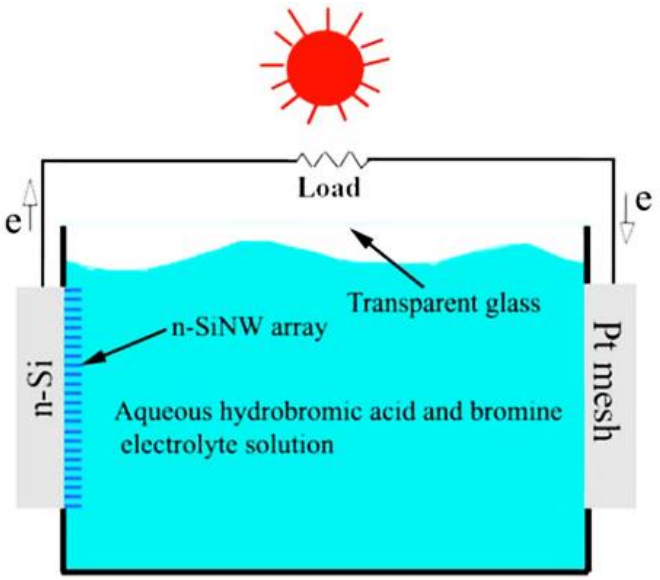

. **Figure 1.3.1:** Schematic presentation of the PEC based on n-SiNW array.

1.3.2 Double-Walled Carbon Nanotubes Used as Counter Electrode[9]

In the year 2009, Shu et al., demonstrated a hybrid heterojunction solar cell consisting of two types of photovoltaic structures, a heterojunction cell and a photoelectrochemical cell connected in parallel as shown in the following figure. The double walled carbon nanotube functions as a transparent and flexible electrode. They have used HBr/Br_2 as a redox electrolyte and the PCE of the cell is 1.29% under 1 sun illumination.

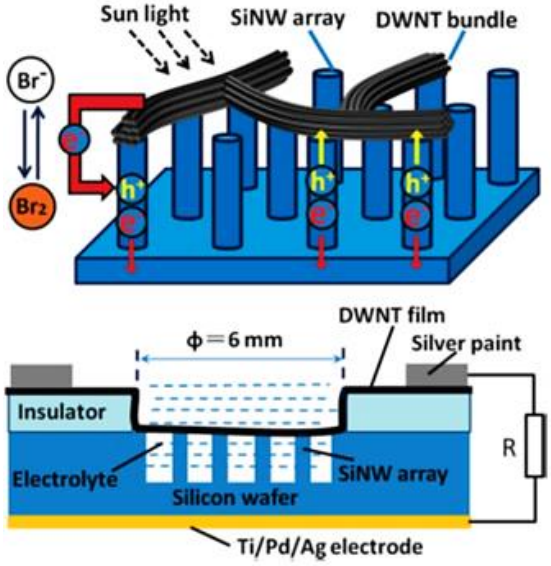

Figure 1.3.2: PEC composed of SiNWs arrays, the DWNT film and the redox electrolyte.

1.3.3 Platinum Nanoparticles for Solar Energy Conversion[10]

In the year 2009, Peng et al., reported a photoelectrochemical cell having platinum nanoparticle decorated silicon nanowire as the photoanode and a platinum mesh as a counter electrode with HBr/Br_2 as a redox electrolyte, showing PCE up to 8.14% under 1 sun illumination. This substantial rise in efficiency was attributed to interfacial charge collecting ability of platinum nanoparticles. They also investigated the effect of Pt NPs deposition time on PEC devices. The PCE was roughly found to be proportional to the number density of Pt NPs. PCE increases with increasing the deposition time up to a certain time and falls after prolonged deposition. Along with Pt NPs they also tried Au NPs decorated SiNW electrode and Ag NPs decorated Si NW electrode in devices. The Au NPs decorated SiNW electrode showed 2.4% efficiency which was lower compared to the Pt NPs decorated SiNW electrode.

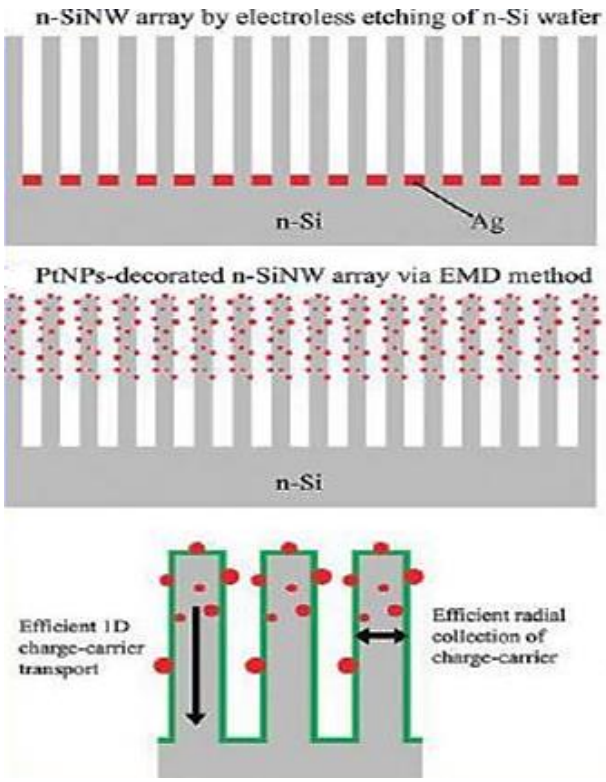

Figure 1.3.3: Graphical presentation of PtNP-decorated n-SiNW arrays prepared by aqueous electroless etching of silicon followed by electroless metal deposition.

1.3.4 SiNW Cell with Passivated & Modified Surface [11]

In the year 2011, Peng et al., reported a photoelectrochemical cell having a carbon coated SiNW electrode as photoanode but they kept the counter electrode and redox electrolyte to be the same as their work in 2009. The cell showed PCE up to 10.86% under 1 sun illumination. In this paper, they addressed the issues of surface passivation and performance degradation

associated with SiNWs PEC. The environmentally friendly and chemically stable ultrathin carbon film passivates silicon nanowire surface and protects them against photocorrosion while Pt nanoparticles further improve the stability of silicon nanowires and lead to significant rise in efficiency due to interfacial charge transfer.

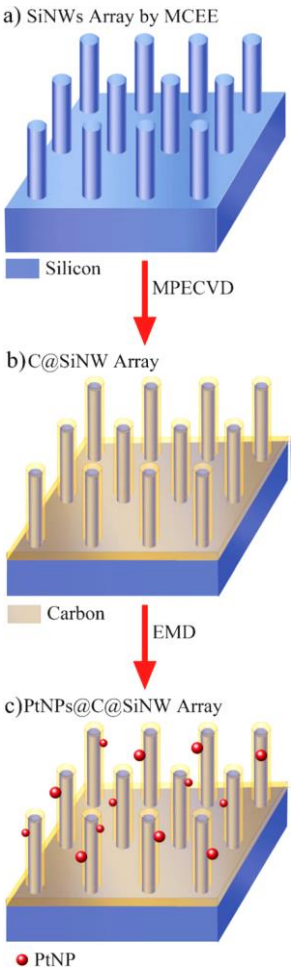

Figure 1.3.4: Schematic illustration of the fabrication process of a PtNPs@C@SiNW array. a) SiNW array prepared by the MCEE method. b) C/Si core/shell nanowire array after carbon MPECVD. c) PtNPs@C@SiNW array after PtNP EMD

1.3.5 Ionic Liquid Electrolyte Based SiNW Solar Cells[12]

In the year 2010, Shen et al., reported a photoelectrochemical cell having LiI/I_2 redox couple dissolved in a mixture of PMII and EMISCN ionic liquid as electrolyte and chemically decorated platinum on ITO glass as a counter electrode and Pt NPs decorated methylated silicon nanowire electrode as photoanode. They methylated the silicon nanowires to passivate the dangling silicon bonds so as to suppress photooxidation and photocorrosion. This cell showed an efficiency = 4.3% under 1 sun illumination. In this paper, they discussed about the

advantages of using ionic liquid as electrolyte solvent. Ionic liquids have some attractive properties such as, good thermal and chemical stability, negligible vapor pressure, non-flammability, high conductivity etc.

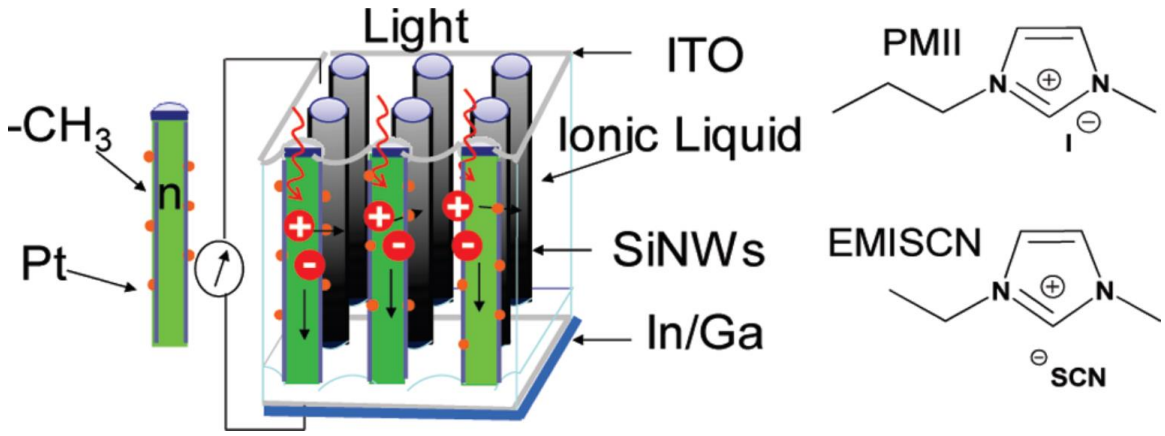

Figure 1.3.5: Graphical presentation of the PEC cell structure using SiNWs as electrode. The vertical SiNWs surface is anchored by methyl groups and decorated with Pt nanodots. The space between SiNWs is filled with electrolyte. Light passes through the top transparent ITO-coated glass electrode.

1.3.6 Aqueous Ferrocyanide/Ferricyanide Redox Electrolyte Based SiNW Cells[13]

In the year 2009, Dalchiele et al., reported a photoelectrochemical cell having a ferrocyanide/ferricyanide redox electrolyte and SiNWs as photoanode and Pt as counter electrode and saturated calomel electrode as reference. The cell showed a PCE = 0.30% under 1 sun illumination.

Table 1.3 Solar cell parameters of liquid junction Si NWs based solar cells reported in literature.

Cell	V_{oc} (V)	J_{sc} (mA cm^{-2})	FF	PCE	Reference
Anode: n-SiNW in HF-$AgNO_3$ for 45 min CE: Pt mesh 3% Br_2 in 40% HBr electrolyte	0.73±0.02	0.872	-----	-----	[6]

Anode: n-SiNW *CE:* DWNT 3% Br_2 in 40% HBr electrolyte	0.5	10.5	0.25	1.29%	[9]
Anode: Pt nanoparticle decorated n-SiNW electrode *CE:* Pt mesh 0.05 M Br_2 in 8.6M HBr electrolyte	0.58	17.2	0.61	6.1%	[10]
Anode: Pt nanoparticle @C @ n-SiNW *CE:* Pt mesh 0.05M Br_2 in 8.6M HBr electrolyte	0.53	36.89	0.55	10.86%	[11]
Anode: Pt nanoparticle decorated methylated SiNW electrode *CE:* chemically decorated Pt on ITO coated glass slides LiI and I_2 in EMISCN and PMII (13:7) mixture electrolyte	0.322	33.7	0.4	4.3% (under 1 sun)	[12]
	0.322	23.2	0.4	6% (under 0.5 sun)	
	0.257	7.8	0.36	4.7% (under 0.15 sun)	
Anode: n-SiNW *CE*: Pt 0.5M KNO_3 + 0.1M $K_3[Fe(CN)_6]$ + 0.1M $K_4[Fe(CN)_6]$	0.323	0.89	0.41	0.30±0.06%	[13]

2. OBJECTIVES OF THIS WORK

- To develop Si NW cells with high efficiency and low recombination losses. This has been accomplished by modifying the anode.
- To explore non-corrosive electrolytes as replacements for HBr/Br_2 (highly corrosive) electrolyte.
- To develop counter electrodes which are low cost, highly conducting as substitutes for costly Pt.

3. EXPERIMENTAL

3.1 Chemicals

Silicon (n-type) wafers were acquired from Siegert wafer. Selenium dioxide (SeO_2), silver nitrate ($AgNO_3$), hydrazine hydrate (H_6N_2O) and isopropanol were purchased from Aldrich. Sulfuric acid (H_2SO_4, 98%), nitric acid (HNO_3, 69%), hydrogen peroxide (H_2O_2, 30%), hydrofluoric acid (HF, 40%), hydrobromic acid (HBr, 47%), ethanol and acetone were purchased from Merck. Bromine (Br_2) was bought from SDFCL. C-fabric was procured from Alibaba Pvt. Ltd and ultra-pure water with a resistivity of $\sim$18.2 MΩ cm was obtained through a Milipore Direct–Q3 UV system.

3.2 Preparation of Trigonal Se[14]

SeO_2 (0.4 g) was dissolved in 20 mL of distilled water and a homogenous solution of selenious acid was prepared under constant stirring. Hydrazine hydrate (0.5 mL) was added slowly to the above solution at room temperature to attain a brick red color indicating the formation of amorphous selenium (a-Se). This solution was further diluted with 20 mL of deionized water and then transferred to a 50 mL stainless steel Teflon lined autoclave. The hydrothermal reaction was maintained at 120 °C for 24 h to obtain trigonal selenium nanoparticles. The black precipitate was isolated by centrifugation, washed thrice with ethanol and distilled water respectively and oven-dried at 60 °C for 6 h.

3.3 Etching of Silicon Wafer[15]

The 1 cm^2 n-Si (100) wafer pieces were initially ultrasonically degreased in acetone and ethanol at room temperature for 10 min. each. The wafer pieces then were immersed in a boiling piranha solution (H_2SO_4: H_2O_2 = 5:2 by volume) for 30 min., and thereafter rinsed in excess deionized water. The cleaned wafer pieces were immediately dipped into a solution of 5 M HF and 0.02 M $AgNO_3$ for 60 min. Thick dendritic coating of Ag wrapped the wafer surface. The vertically aligned SiNW arrays were obtained after the wafer was immersed in a bath of concentrated nitric acid for 10 min., to remove the residual Ag layer. A black Si NWs etched

silicon wafer was acquired which was then washed in deionized water to remove the acid residue followed by the removal of oxide layer with buffered hydrofluoric acid solution (H_2O: HF = 50:1 by volume) and dried under ambient conditions.

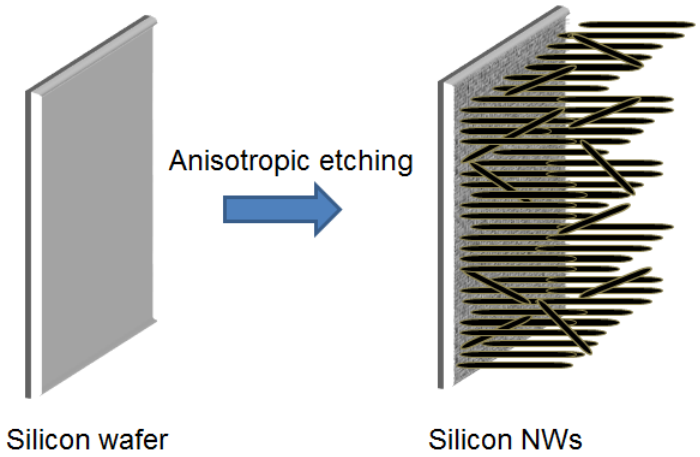

Figure 3.3: Schematic presentation of vertically aligned silicon NWs after anisotropic etching.

3.4 Photovoltaic Device Fabrication[16]

As synthesized t-Se were dispersed in isopropanol and deposited over the etched nanowires on Si wafer by drop-casting to customize the photoanode for the solar cell. Highly conducting carbon fabric was chosen as counter electrode and the aqueous electrolyte comprised of 8.6 M HBr and 0.05 M Br_2 as the redox mix.

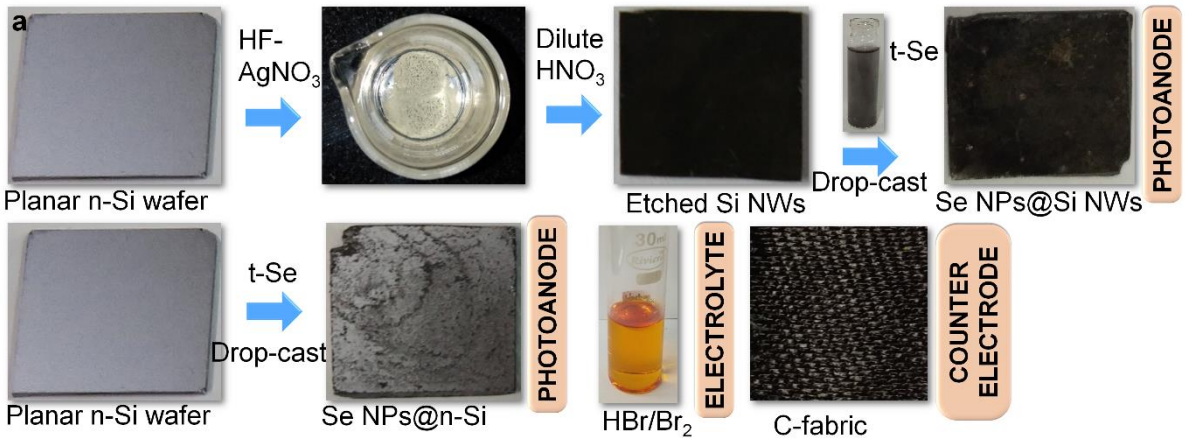

Figure 3.4(a): Illustration of Fabrication of Si NWs, Se NPs@Si NWs, and Se NPs@ n-Si Photoanodes through Photographs

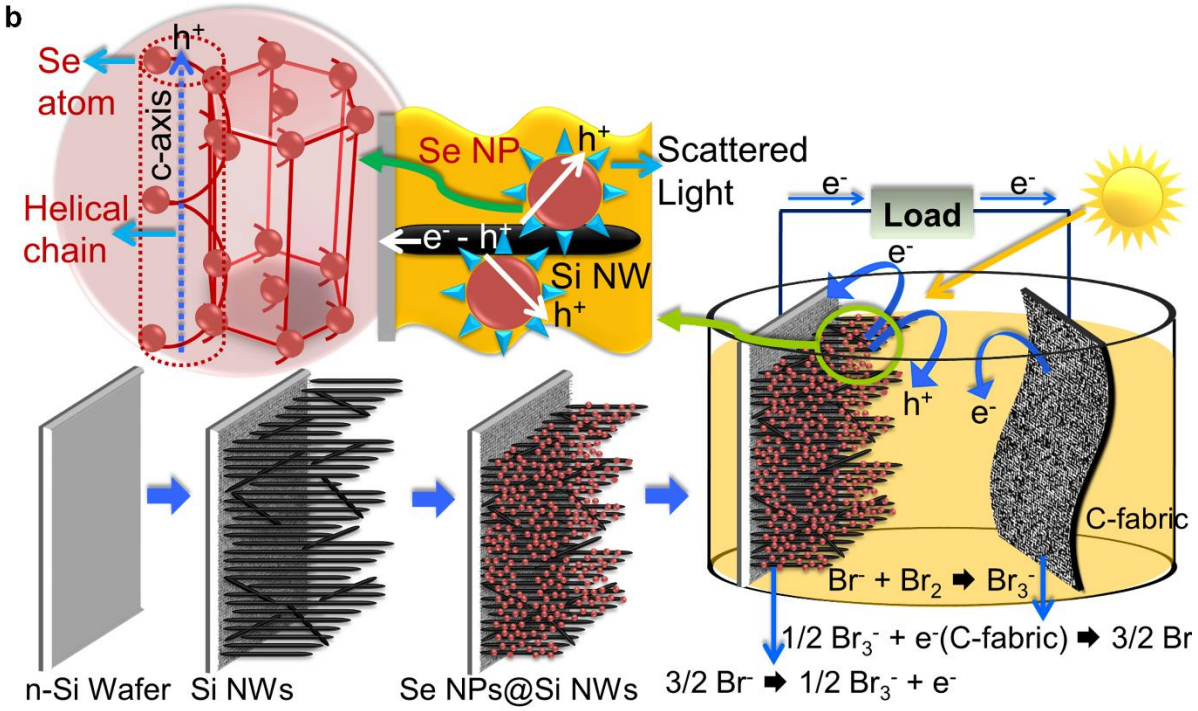

Figure 3.4(b): Schematic of the Preparation of Se NPs@Si NWs and the Liquid-Junction PEC Solar Cell.

4. RESULT AND DISCUSSION[16]

4.1 STRUCTURAL CHARACTERIZATION

4.1.1 SEM Analysis

The surface morphology analysis was performed using Field Emission Scanning Electron Microscopy (FE-SEM; Carl Zeiss Supra 40). A very dense network of SiNWs obtained by metal assisted electroless etching of Si wafer which can be evidenced from SEM images of SiNWs. The diameters of the wires vary from 60 to 250 nm, and their average length is about 10 µm. The vertically aligned SiNWs with respect to the Si wafer can be clearly observed from the top view SEM images of SiNWs. The image is consistent with previously observed images of Si NWs prepared by an etching process.[10] The uniform distribution of Se NPs across the lengths of SiNWs can be observed from figure 4.1.1(e-f). The particle density is much higher in this case compare to pristine SiNWs and Se NPs tend to fill the gaps between the individual wires. The SEM image of Carbon fabric which is used as counter electrode for this liquid

junction solar cell is shown in figure 4.1.1(h). It shows overlapping smooth fibers of carbon, which impart the fabric like texture to this free standing flexible electrode.

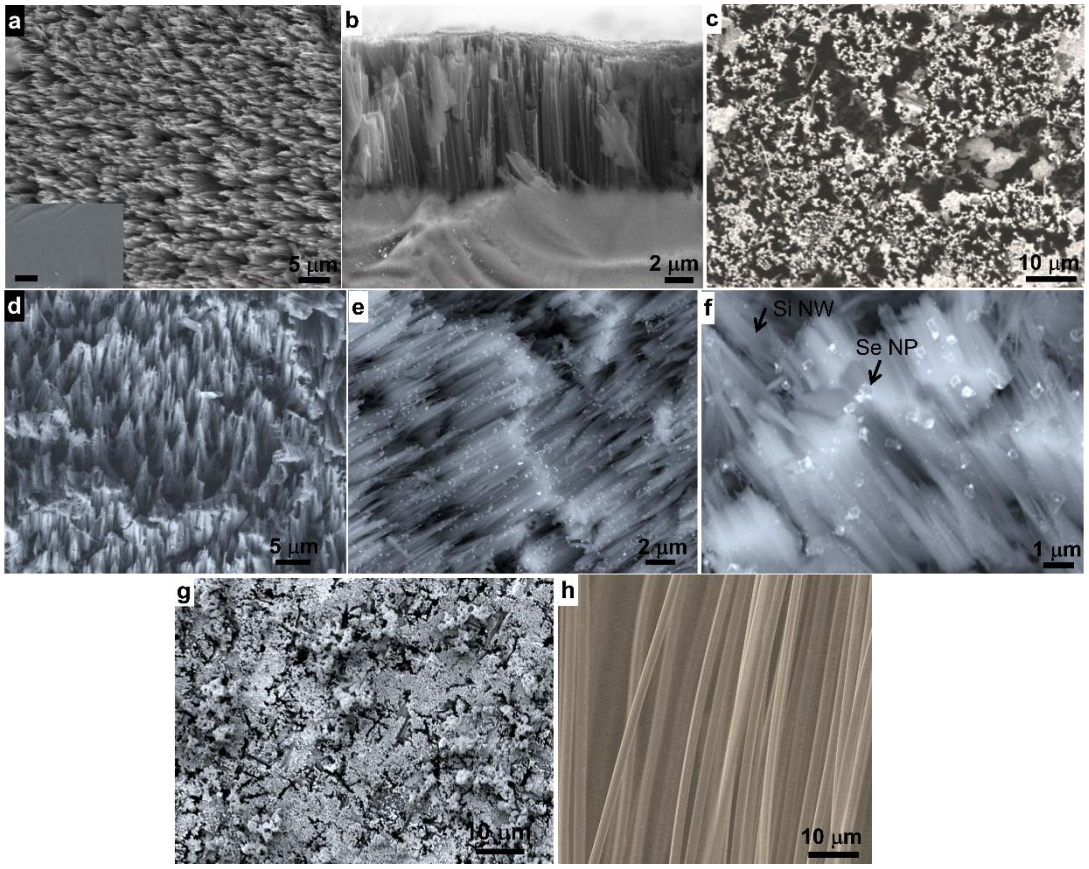

Figure 4.1.1: SEM image of **(a)** SiNWs; inset shows the image of an n-Si wafer **(b)** Cross sectional view **(c)** top view of SiNWs **(d)** dense network of SiNWs **(e-f)** SeNPs@SiNWs **(g)** top view of SeNPs@SiNWs **(h)** C fabric.

4.1.2 TEM Analysis

Transmission Electron Microscopy (TEM) images were obtained for trigonal selenium on a JEOL 2100 microscope operating at an accelerating voltage of 200kV. From the TEM image shown in figure 4.1.2(a) proves the presence of Se NPs. The diameter of spherical Se NPs varies from 40 to 80 nm. The selected area electron diffraction (SAED) shows spotty concentrated rings which confirms polycrystalline nature of Se NPs. Some of the bright spots are indexed to the (100), (101), (112) and (210) planes of hexagonal Se.

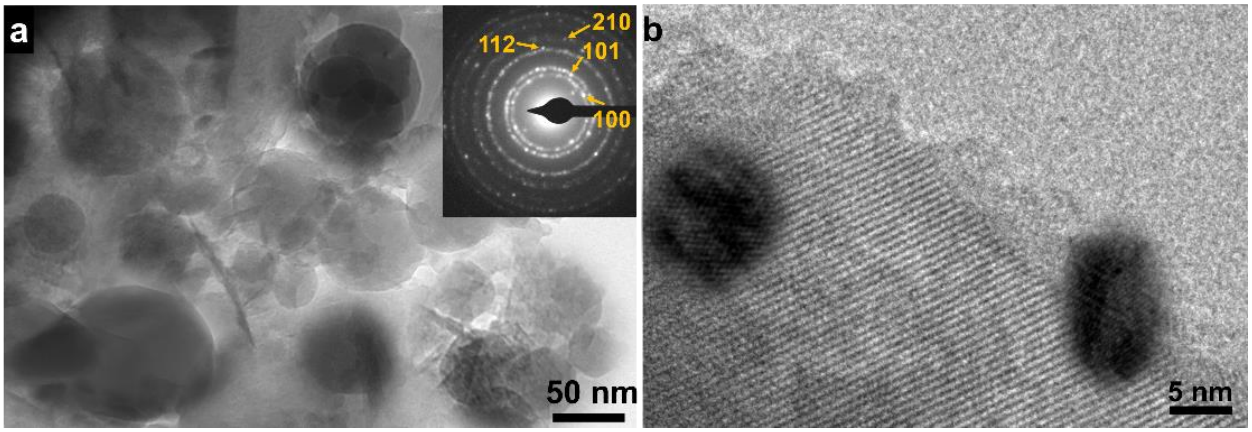

Figure 4.1.2: (a) TEM image of Se NPs; inset shows the SAED pattern **(b)** HRTEM of SeNPs@SiNWs.

4.1.3 Raman Analysis

Raman spectra were recorded on a Bruker Senterra dispersive Raman microscope spectrometer, with a 532 nm laser excitation. Raman spectra of SiNWs and SeNPs@SiNWs are shown in figure 4.1.3. An intense peak observed at 523 cm^{-1} which can be assigned to Si-O bond vibration of SiNWs etched wafer.[17] For SeNPs@SiNWs an additional peak observed at 235 cm^{-1} which is due to A1 symmetric vibrational stretching mode of the Se-Se bonds characteristic of helical Se chain in trigonal(t) phase.[18]

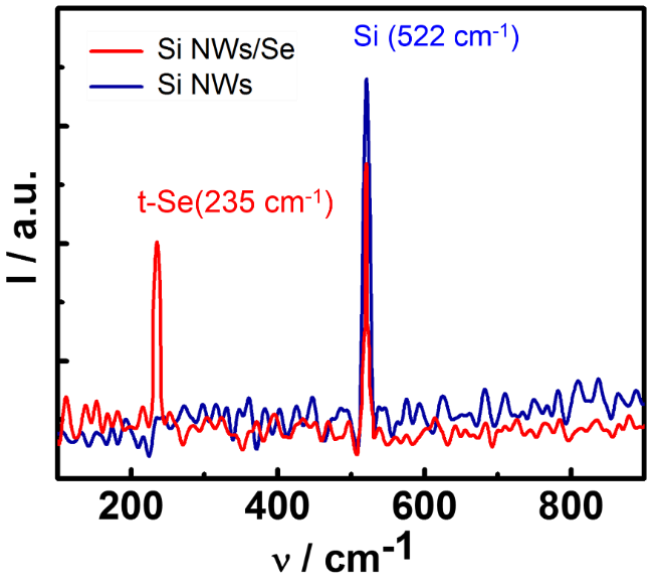

Figure 4.1.3: Raman Spectra of SeNPs@SiNWs and SiNWs.

4.1.4 XRD Analysis

XRD patterns recorded for the Se NPs, Si NWs etched wafer and Se NPs@ Si NWs are shown in the following Figures. The most intense peak for crystalline trigonal Se is observed at 2θ =

29.70^0 followed by peaks at 43.64^0, 23.51^0, 51.71^0, 45.35^0, 41.30^0, 56.13^0, 65.23^0, 61.65^0, 71.58^0, 68.25^0 aligning with d = 3.00, 2.07, 3.78, 1.76, 1.99, 2.18, 1.63, 1.42, 1.50, 1.32, 1.37 Å corresponding to the (101), (102), (100), (201), (111), (110), (112), (210), (202), (113), (211) planes of the hexagonal crystal structure as per JCPDS card no. 060362.In the XRD spectra of Se NPs no peaks of SeO_2 or any other impurities is observed, hence the sample is pure. The lattice constants obtained are a = 4.366Å and c = 4.953Å which proves the presence of trigonal Se NPs. A highly intense peak at $2\theta = 69.14^0$ observed in the diffraction patterns of Si NWs and Se NPs@ Si NWs matching with d = 1.36 Å corresponds to the (400) plane of the face centered cubic (fcc) crystal lattice (JCPDS: 892955) which is parallel to the (100) plane of n-Si wafer. The pattern of Se NPs@ SiNWs NWs clearly shows peaks corresponding to both pristine t-Se and Si.

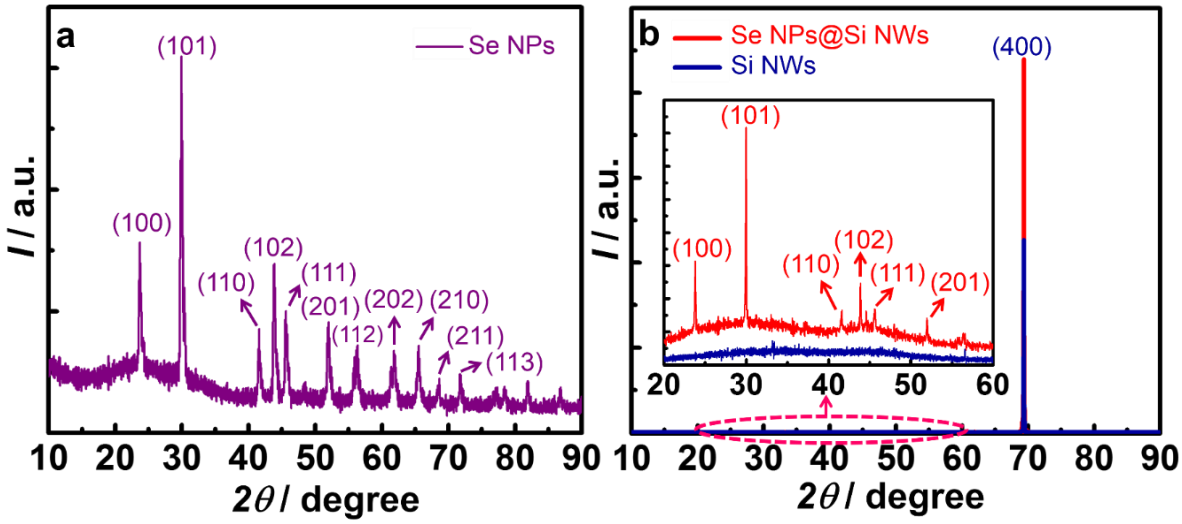

Figure 4.1.4: XRD patterns of **(a)** Se NPs **(b)** SeNPs@SiNWS; inset is an enlarged view of low 2θ region.

4.1.5 AFM Analysis

AFM topography images were recorded on using a Veeco, Multimode 8 with scan Asyst (Nanoscope 8.10 software) microscope. The Si tip with a cantilever of antimony (n)-doped Si is used for recording the surface images. The AFM topography images of SiNWs shows the presence of smooth nanowires where as for SeNPs@SiNWs the presence of Se NPs over SiNWs can clearly observed. The root mean square surface roughness for the two samples is 56.45 and 90.32 nm respectively. Thus SeNPs increases the surface roughness of the electrode.

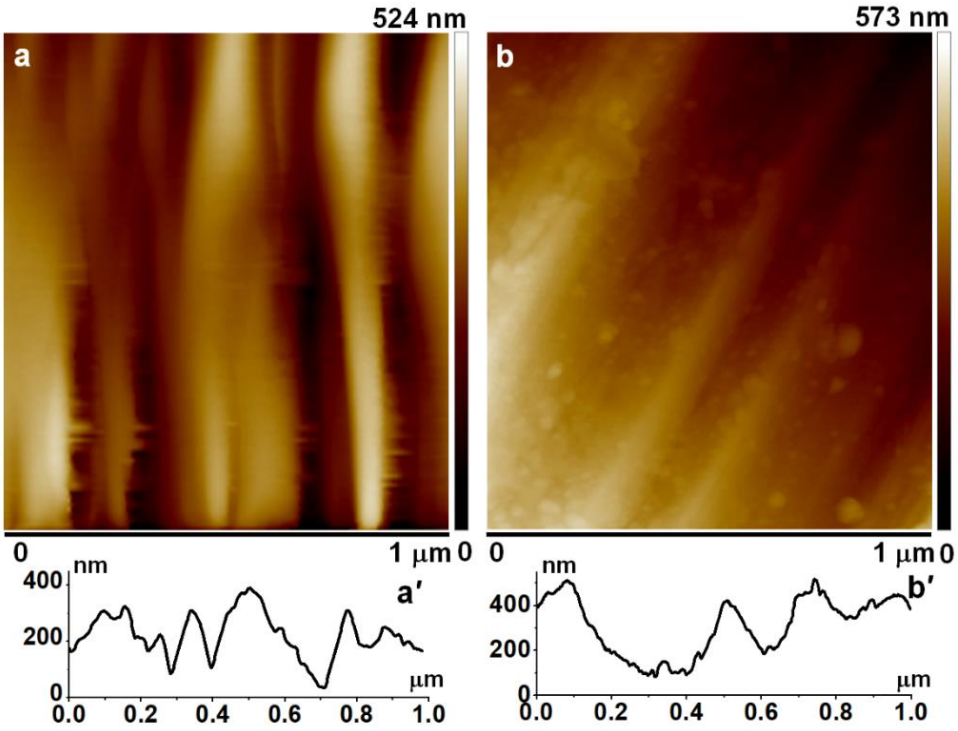

Figure 4.1.5: AFM topography images and section profiles of (a, a′) SiNWs (b, b′) SeNPs@SiNWs

4.2 OPTICAL CHARACTERIZATION

4.2.1 Absorption Spectral Analysis

The optical absorption spectra were measured in the diffuse reflectance mode and converted to absorbance using the Kubelka−Munk function on a UV−VIS−NIR spectrophotometer equipped with an integrating sphere (Shimadzu UV-3600). The absorption spectra of SiNWs, Se NPs and Se NPs@ SiNWs are shown in the following figure. Se NPs exhibit an absorption band in the 400 to 700 nm wavelength span and the band gap is calculated to be 1.69 eV from its absorption edge. The absorption band of Si NWs is broader extending over the visible and NIR region from 400 to 1000 nm, and then it tapers off. The band gap calculated from the absorption edge is 1.16 eV for n-Si. Se NPs @Si NWs absorbs over both visible and NIR regions, with an enhanced absorption compared to pristine Si NWs, particularly over the 400 to 650 nm span. The scattered light from Se in this region enhances the charge carrier excitation in SiNWs causing electron-hole separation.

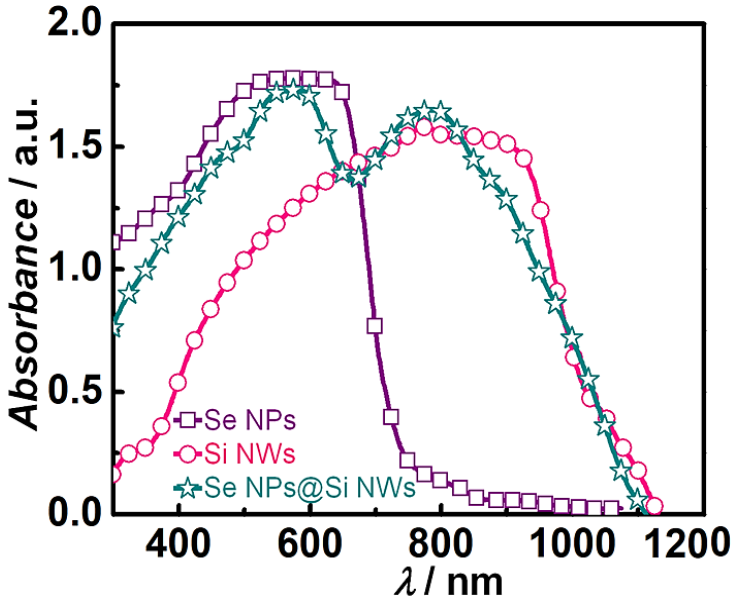

Figure 4.2.1: Absorbance spectra of SeNPs, SiNWs and SeNPs@SiNWs.

4.2.2 Diffuse Reflectivity Spectral Analysis

The optical absorption spectra were measured in the diffuse reflectance mode on a UV−VIS−NIR spectrophotometer equipped with an integrating sphere (Shimadzu UV-3600). The average reflectivity of planar Si wafer is ∼37% whereas that of Si NWs is only ∼5% in the 300–1100 nm wavelength range which is because of the superior antireflectivity property of SiNWs compared to Planar Si. The scattered light from the rough surface of individual SiNW gets trapped inside the dense network and consequently lowering light transmittance or reflectance.

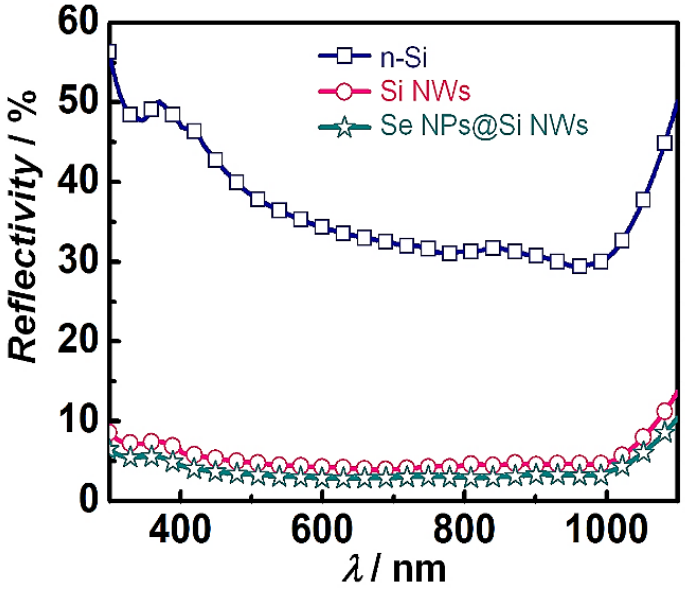

Figure 4.2.2: Variation of reflectivity of n-Si, SiNWs, SeNPs@SiNWs with wavelength.

4.3 PHOTOELECTROCHEMICAL CHARACTERIZATION

4.3.1 Photoconductivity Measurement

Conductance (G) was measured by linear sweep voltammetry (LSV) using two FTO glass electrodes for sandwiching the t-Se powder with a 2 mm wide para-film spacer in between, over a voltage window of -2 to +2V.The I-V profiles are found to be linear hence showing ohmic behavior and the conductivity(κ) of Se NPs, is deduced from the slopes of the linear fits, as per the relation: $\kappa = \Delta I/\Delta V$ (d/a), where 'd' is the thickness of the spacer or the sample and 'a' is the sample's cross-sectional area. The dark conductivity and the photoconductivity are 41.1 and 381.6 μS cm^{-1}. This result proves the photoconductive nature of P type Se NPs under illumination.

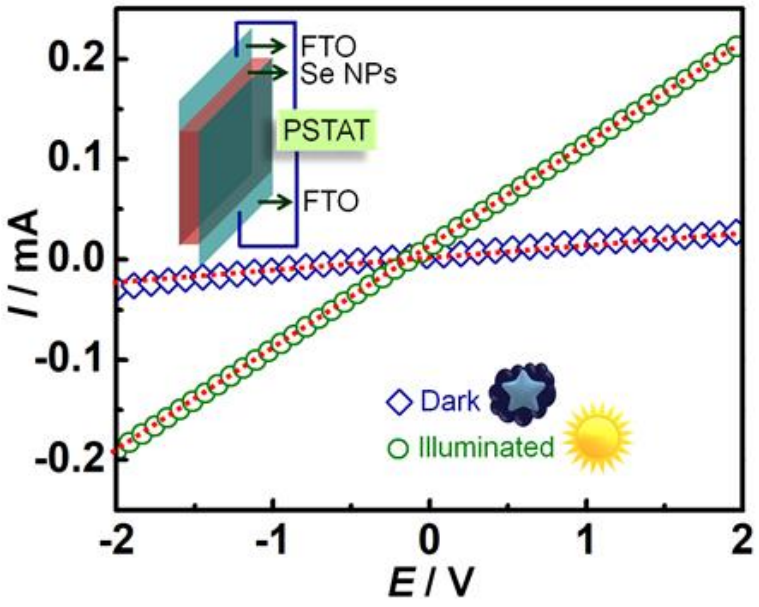

Figure 4.3.1: J-V plots of SeNPs recorded under 1 sun illumination.

4.3.2 Mott-Schottky Plot of Se NPs

Mott-Schottky plot for the SeNPs were recorded on an Autolab PGSTAT 302N equipped with a frequency response analyzer (FRA) and a NOVA 1.11 software, under an AC amplitude of 1V. The P-type nature of Se NPs is confirmed using mott-schottky plot. The plot of $1/(\text{capacitance})^2$ Vs voltage (V) gives a negative slope. Hence the P type nature of SeNPs can be confirmed. The equation from which the density of holes calculated is-$1/C^2 = 2/e\varepsilon_r\varepsilon_o N [E-E_{fb} - \kappa T/e]$ So, the slope is = $2/e\varepsilon_r\varepsilon_o N$. The known value of ε_r or the dielectric constant of hexagonal Se from an earlier report is 8.1.[19] Hence, hole density (N) is found to be $5.06*10^{16}$ which is close to a value of 10^{15} cm^{-3} known from an earlier report.[20]

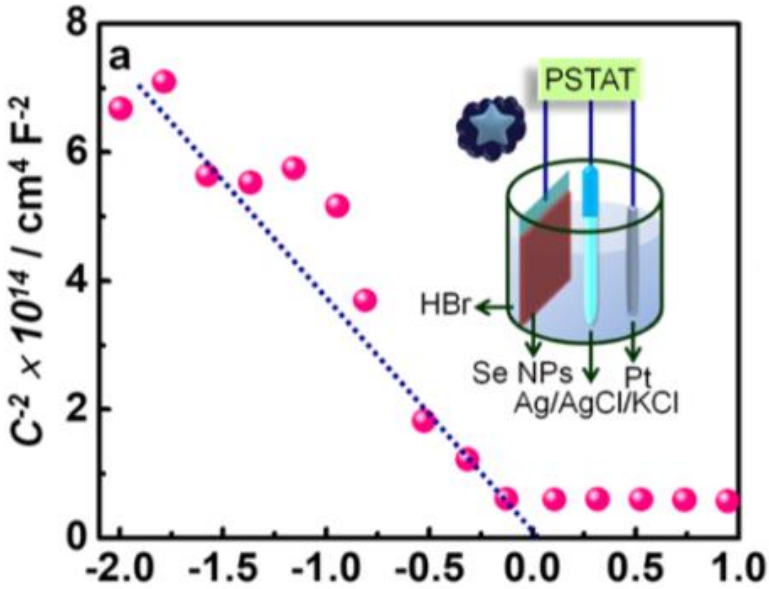

Figure 4.3.2: Mott-Schottky plot of Se NPs recorded in dark.

4.3.3 Cyclic Voltammetry

Cyclic voltammetry (CV) was performed under three electrode system with Pt as the CE, and Ag/AgCl/KCl used as a reference electrode in an aqueous 0.1 M KCl electrolyte solution on an Autolab PGSTAT 302N equipped with a NOVA 1.9 software at a scan rate of 20 mV s^{-1}. In each case, a reduction peak was observed in the cathodic sweep, which can be equated to the CB or the Lowest Unoccupied Molecular Orbital (LUMO) position of the sample and similarly for anodic sweep the observed oxidation peak can be assigned to VB or Highest Occupied Molecular Orbital (HOMO). This is explained in the following Figures. The electrode potential of the reference is +0.197 V, which is added to the Ered vs. Ag/AgCl/KCl to obtain the Ered vs. NHE (normal hydrogen electrode) of the respective working electrodes. The Ered vs. NHE in volts was subtracted from -4.5 eV (≡ 0 V versus NHE) in order to convert this value to eV. The band positions(eV) obtained from cyclic voltammetry are summarized in the following table.

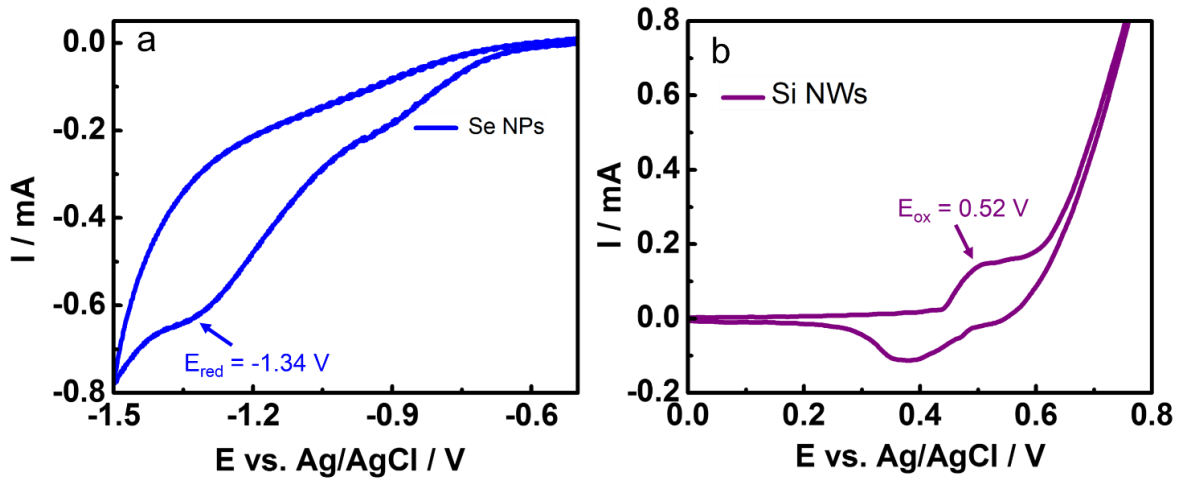

Figure 3.3.3: cyclic voltammetry of **(a)** SeNPs **(b)** SiNWs.

The HOMO (VB), LUMO (CB) and band gap values of Si and Se used in cell fabrication were acquired from cyclic voltammograms and absorbance spectra using the equations provided below.

$$E_{red} = -4.5 \text{ eV}(\equiv 0 \text{ V } \textit{versus} \text{ NHE}) - (\text{Red. Peak (V) vs. Ag/AgCl/KCl} + 0.197 \text{ V}) \quad (1)$$

$$E_{ox} = -4.5 \text{ eV } (\equiv 0 \text{ V } \textit{versus} \text{ NHE}) - (\text{Ox. Peak (V) vs. Ag/AgCl/KCl} + 0.197 \text{ V}) \quad (2)$$

Table 3.3.3: Energy level positions of the photoanode components.

Material	Reduction peak / V vs. Ag/AgCl	Oxidation peak / V vs. Ag/AgCl	E_{red} (versus NHE) / eV ≡ LUMO	Band Gap / eV	E_{ox} (versus NHE) / eV ≡ HOMO
Si NWs	…….	0.519	-4.046	1.16	-5.247
Se	-0.787	…….	-3.356	1.69	-5.046

4.3.4 Energy Profile Diagram

The energy band diagram for SeNPs @SiNWs showing all possible electron transfer modes on illumination, is illustrated in Fig 3.4. The positions of VBs and CBs of the different components used in the diagram were determined from cyclic voltammograms and absorption spectra. Under illumination electronic excitation takes place in both SiNWs and Se NPs. Both the valence band(VB) and conduction band(CB) of SeNPs is higher in energy compare to SiNWs. Electrons from CB of SeNPs are transferred to CB SiNWs from which it is transported through external circuit to counter electrode where it reduces the oxidized species Br_3^- to Br^-. The

generated holes in the VB of SiNWs are transferred to SeNPs which acts as efficient hole transporter and oxidizes the reduced species Br^- to Br_3^- and thereby completes the cycle.

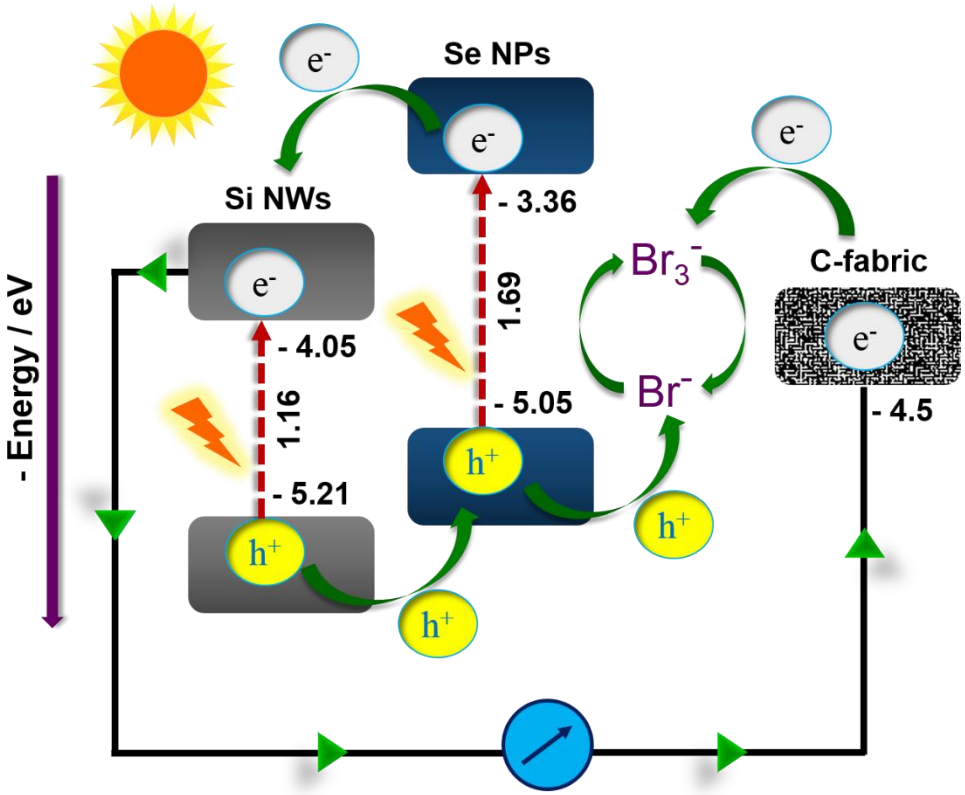

Figure 4.3.4: Energy level diagram of the SeNPs@SiNWs-Br^-/Br_2-C fabric solar cell showing all possible modes of electron transfer under 1 sun illumination

4.3.5 Solar Cell Characterization

Current versus potential (I−V) data of solar cells were measured using a LOT-Oriel solar simulator coupled with a Metrohm Autolab PSTAT302N. The light source was a 150 W Xenon arc lamp, which delivered a collimated output beam of 25 mm diameter through Air Mass (AM) 1.5 filter, providing a light intensity of 100 mW cm^{-2} (1 sun).

Table 4.3.5: Solar cell parameters of cells with 8.6 M HBr/0.05 M Br_2 aqueous solution electrolyte and C-fabric counter electrode under 1 sun illumination (100 mW cm^{-2}) are listed with the photoanodes (exposed cell area ~0.5 cm^2).

Photoanode configuration	V_{OC} (mV)	J_{SC} (mA cm^{-2})	FF (%)	η_{best} (%)	η_{avg} (%)
n-Si	426	0.41	27.42	0.048	0.041

SeNPs@n-Si	479	0.69	28.05	0.092	0.087
Si NWs	734	13.88	48.23	4.912	4.42
SeNPs@Si NWs	790	17.12	51.96	7.028	6.75

The n-Si photoanode shows a best cell efficiency 0.048 which is almost doubled to 0.092 when SeNPs dropcasted over n-Si. This is mainly because of the photoconductive nature of Se NPs which leads to better charge transport. The other solar cell parameters like V_{oc}, J_{sc} and FF shows slight increase compare to planar Si. But when the planar Si is replaced by etched SiNWs electrode the cell performance improves dramatically. The best cell efficiency is 4.912 which is almost 100 times and short circuit density rises almost 30 times compare to planar Si. These are mainly because of beneficial optical and structural properties of SiNWs. But when Se NPs are dropcasted over SiNWs the efficiency rises up to 1.5 times and open circuit voltage increases by 60 mV. This is mainly because of the hole transporting property of the P type Se NPs.

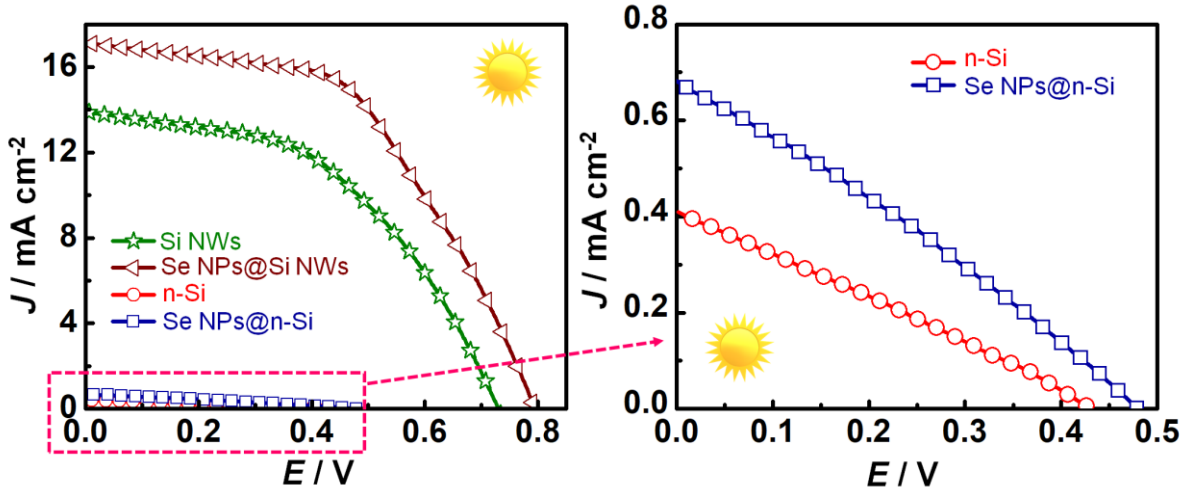

Figure 4.3.5: J-V characteristics of liquid junction PEC solar cells with different photoanodes, C fabric as the CE, and Br^-/Br_2 as the electrolyte under 1 sun irradiance (AM1.5).

4.3.6 IPCE Measurement

Incident photon conversion efficiency (IPCE) versus wavelength was measured on a Newport machine with a tunable Xe lamp (300W) as the light source. IPCE measurement were performed using SiNWs and SeNPs@SiNWs as photoanode respectively having C fabric as

counter electrode and 0.05M Br_2 in 8.6M HBr solution as the electrolyte in both cases. The SiNWs/Br_2/Br^-/C fabric cell configuration gives maximum IPCE of 51.7% at λ= 600 nm. But when SeNPs is tethered on SiNWs IPCE increased up to 62.2%. Both the curves tapered off to zero at 1100 nm. IPCE mainly depends on the electron ejection and photon collection efficiency and light absorption by photo anode. SeNPs being a P type hole transporting material favors radial junction hole collection and thereby reducing recombination and increasing IPCE compare to SiNWs over the entire range of solar spectrum under consideration. Also in terms of light harvesting Se NPs has a broad absorption peak in 350-630 nm range and thus the dependence of IPCE of SeNPs tethered SiNWs cell on light absorption property of SeNPs can be observed. Se NPs can act as a light scattering material as well which is mainly attributed to the diameter of the nanoparticle. Here the diameter of Se NPs mainly varies from 40-80 nm and the average cluster of Se NPs is large enough and ideally it should be more than 50 nm for absorption to take place predominantly. Hence light scattering process of SeNPs cannot be ignored. Also scattering and absorption are not mutually independent process, these may occur simultaneously. The scattered light from SeNPs causes electronic excitation in SiNWs helping electron-hole separation. Thus IPCE enhancement for SeNPs tethered SiNWs cell is because of both light scattering and absorption.

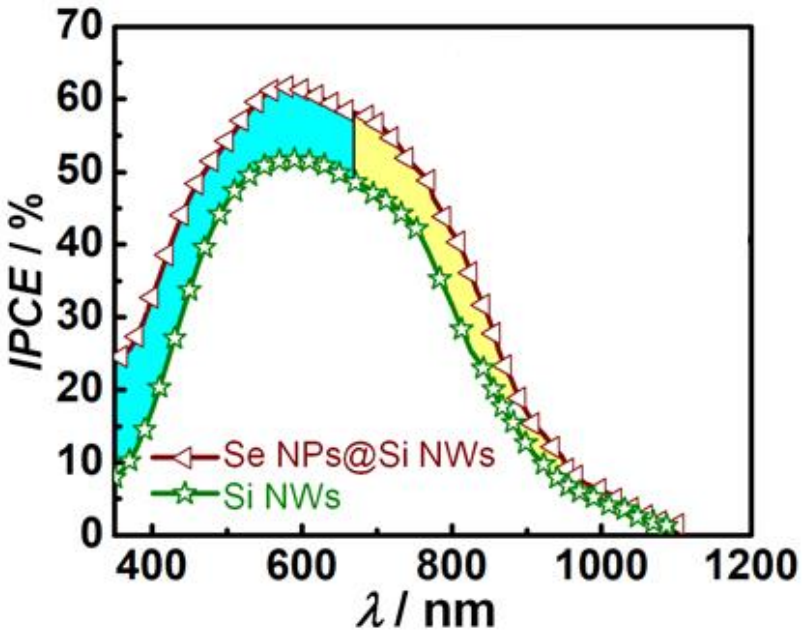

Figure 4.3.6: IPCE vs wavelength curves for the solar cells with Se NPs@Si NWs and Si NWs photoanodes.

4.3.7 Impedance Studies

Impedance measurements were performed on Autolab PGSTAT 302N. The Nyquist plots were generated over a frequency range of 1 MHz to 0.01 Hz, by applying an ac potential of 20 mV over the open circuit potential in dark as seen in Fig 3.3.6(a, b). These plots display a skewed semicircle, followed by an incomplete arc and these plots are fitted in to the [R(RQ)(RQ)] equivalent circuit as shown in the following figures. The charge transfer resistance in case of planar Si wafer is higher compare to SiNWs (>30 KΩ). Recombination resistance, Rrec is inversely proportional with the recombination rate of electrons in Si with the oxidized redox species charge of redox electrolyte at the electrolyte-electrode interface. The diameter of the skewed semicircle in the mid- to low frequency range represents R_{rec}. The EIS parameters obtained from the fits are tabulated in table 4.3.7. The R_{rec} value for Se NPs@Si NWs/Br^-/Br_3^-/C-fabric cell is1.7 kΩ and for bare Si NWs, the value drops to 1.11 kΩ which is due to the presence of P type hole conducting Se NPs in the former cell configuration. R_{rec} being sensitive to surface processes, exhibits a strong dependence on illumination owing to the presence of photo generated charge carriers (Figure 3.3.6 c). Under illumination though the R_{rec} of SeNPs@SiNWs decreases to 0.97 KΩ but this is dominated by the facile hole transporting property of SeNPs which reduces the series resistance leading to an effective charge transport at the electrode-electrolyte interface.

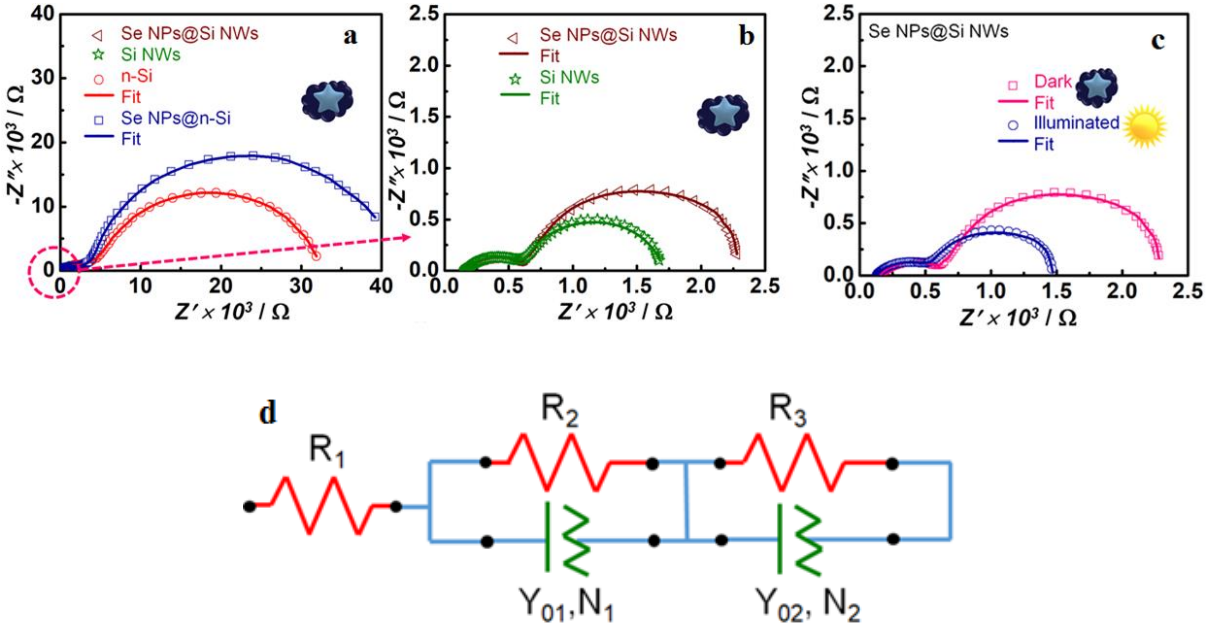

Figure 4.3.7: Nyquist plots of (a, b) solar cells with photoanode- Br^-/Br_2-C fabric with varying photoanodes in dark, over a frequency range of 10^6 to 0.1 Hz at V_{OC} and (c) solar cell with the SeNPs@SiNWs as photoanode under dark and under irradiance (50 $mwcm^{-2}$) at V_{OC}.(d) equivalent circuit used for fitting the data.

Table 4.3.7: EIS parameters obtained from the fitted Nyquist plots of liquid junction PEC solar cells with different photoanodes.

Photoanode	R_1 (Ω)	R_2 (KΩ)	Y_o ($\mu\Omega^{-1}$)	N_1	R_3 (KΩ)	Y_o ($\mu\Omega^{-1}$)	N_2
n-Si	160.7	2.65	1.08	0.93	30.02	2.45	0.91
Se NPs@n-Si	145	2.27	1.26	0.92	36.38	1.94	0.95
Si NWs	159.5	0.43	4.95	0.61	1.09	31.2	0.92
Se NPs@Si NWs	157	0.42	6.67	0.70	1.69	27.45	0.92
Se NPs@Si NWs (light)	129	0.37	8.22	0.61	0.97	34.9	0.93

4.3.8 Transient Photovoltage Decay Analysis

Photovoltage decay versus time measurement was carried out by using a 1 sun white light source coupled to an Autolab PGSTAT 302N, which recorded the chronopotentiometric data in dark. Transient photovoltage decay plots are measured in the dark after attaining a stable voltage under a white light irradiance of 100 $mWcm^{-2}$ (Figure 4.3.8). The photovoltage decay duration is proportional to open circuit voltage(V_{OC}). Hence this decay duration is proportional to charge built up in the photoanode which is equivalent to inbuilt potential. So greater the charge built up in the photoanode greater will be the photovoltage decay duration. The photovoltage decay duration is also representative of back electron transfer to oxidized couple of the redox electrolyte from CB of Si. So greater the photovoltage decay duration lower will be charge recombination. The normalized photovoltage decay time obtained for SiNWs is 30 ms where as for SeNPs@ SiNWs it is 42 ms. There for we can say that in presence of hole transporting material like Se NPs over the SiNWs the recombination is lowered due to facile hole propagation which helps in rise in V_{OC} where as for Pristine SiNWs the excited charge carriers easily recombine to the oxidized couple of redox electrolyte causing a comparatively low V_{OC}. The Se NPs in 400 nm to 650 nm region of the spectra acts as light scattering material also. This scattered light causes charge carrier excitation in photoanode which in turn gives rise to greater photovoltage. Again in this study the redox electrolyte used is HBr/Br_2 which is highly corrosive in nature thus the formation of insulating oxide layers over the photoanode

surface cannot be ignored which causes in lowering in charge built up and V_{OC}. Therefore, the greater photovoltage decay duration incase of SeNPs@ SiNWs can be justified.

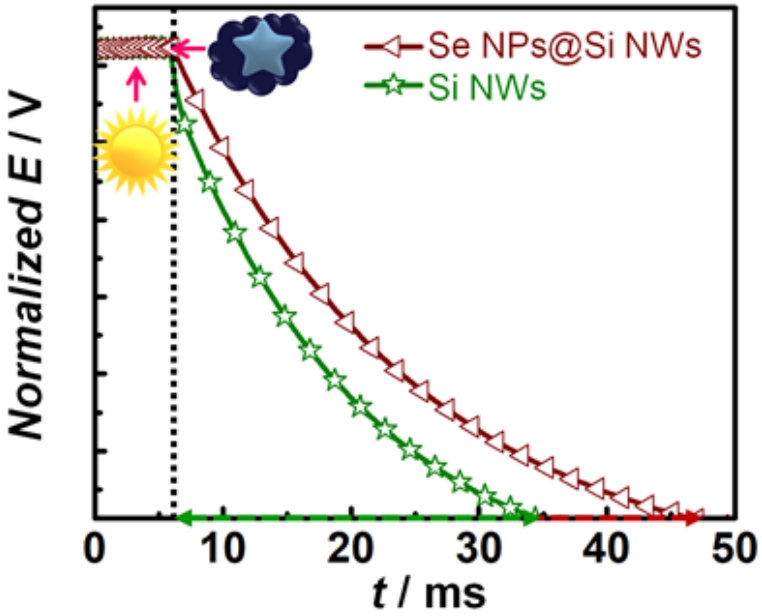

Figure 4.3.8: transient photovoltage decay plot of SeNPs@SiNWs and SiNWs.

4.3.9 Transient Photocurrent Analysis

Photocurrent versus time measurement was carried out by using a 1 sun white light source coupled to an Autolab PGSTAT 302N, which recorded the chronoamperometric data in dark. The highest photocurrent delivered by the Si NWs based cell is 14 mA cm^{-2} which rapidly decays under initial irradiation time. The stabilized photocurrent then attained after a few seconds is ~7 $mAcm^{-2}$. The Se NPs@Si NWs cell shows a maximum response of 17 mA cm^{-2} which also drops to a stable value of ~11 mA cm^{-2} but the decay is comparatively slower than that of Si NWs cell. The faster photocurrent decay in case of SiNWs based cell is mainly because of the oxidation caused by the corrosive HBr/Br_2 electrolyte on the surface of silicon nanowire which in turn increases series resistance of cell. But when SiNWs surface is decorated by Se nanoparticles it passivates the SiNWs surface thereby reducing photooxidation and series resistance. Photooxidation mainly happens because of the reaction between generated hole in valence band with the atoms on the surface in this case it is silicon. But when hole conductive

material like Se NPs is present it passivates the SiNW surface and prevents photooxidation. This is why the photocurrent decay incase of Se NPs @SiNWs is slow.

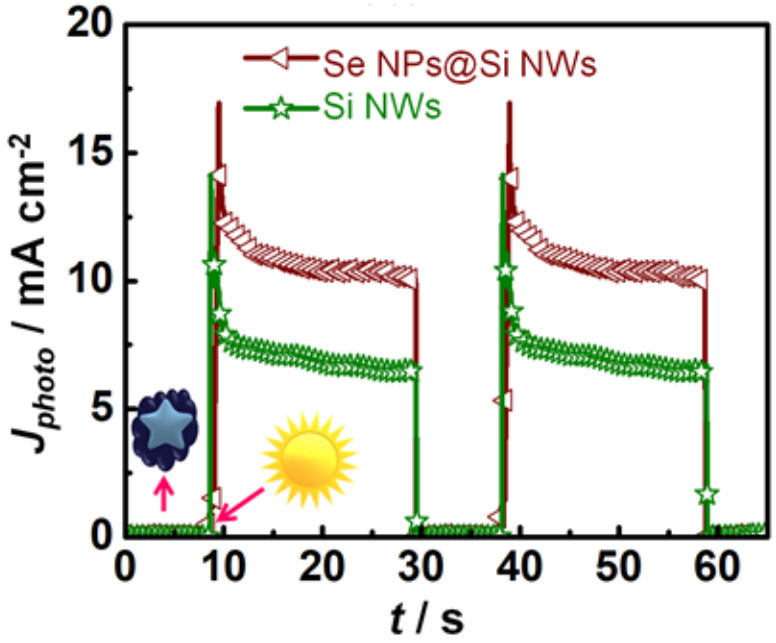

Figure 4.3.9: transient photocurrent decay plot of SeNPs@SiNWs and SiNWs.

4.3.10 Solar Cell Stability

Table 4.3.10: Effect of prolonged continuous 1 sun illumination on a cell with Se NPs@Si NWs/Br^-/Br_3^-/C-fabric configuration (active area ~0.5 cm^2).

Illumination	Voc (mV)	Jsc (mA cm^{-2})	FF (%)	PCE (%)
0 h	778	16.90	52.86	6.95
1 h	772	16.74	49.82	6.44
2 h	756	15.97	45.61	5.51
3 h	724	14.84	45.30	4.87
4 h	687	10.37	44.35	3.16
5 h	661	9.29	43.97	2.70
6 h	655	8.16	43.59	2.33

The open circuit voltage (V_{OC}) of the solar cell remained almost same for 6h as only 100mV reduction could be observed. But the short circuit current density (J_{SC}) become less than half of the initial value. This is possibly because of the photooxidation or photocorrision happening

inside the cell. Although the open circuit voltage remained almost same but due to huge drop in current the power conversion efficiency(PCE) become almost one third of its initial value.

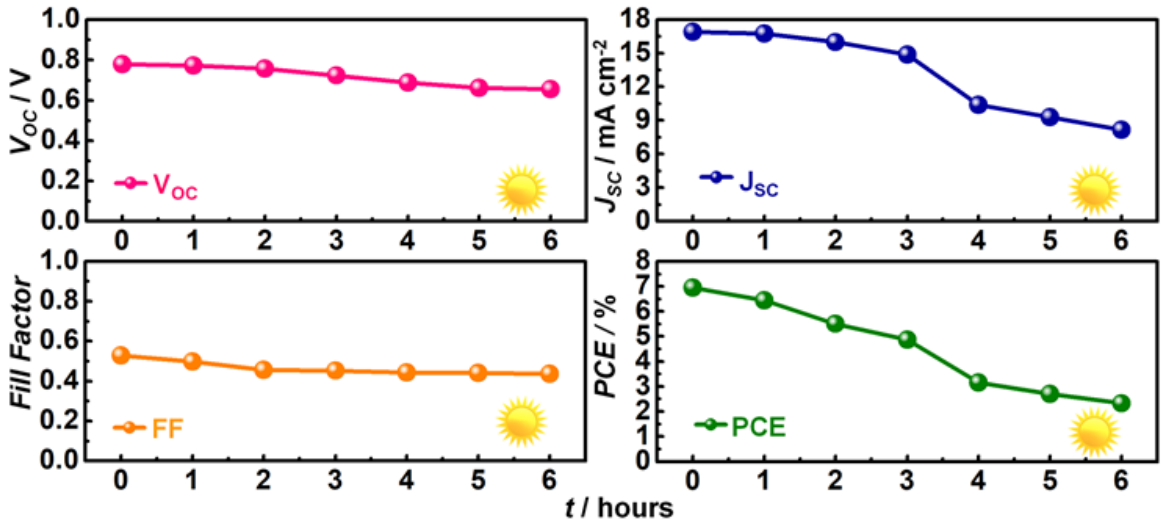

Figure 4.3.10: Effect of 1 sun exposure (100 mwcm^{-2}) on cell parameters: V_{OC}, J_{sc}, FF, and PCE of SeNPs@SiNWs/Br^-/Br_3^-/C fabric solar cell on continuous illumination for 6h.

4.3.11 Control cell experiment

A comparative study has been done between SeNPs@ SiNWs based device and a control cell architecture which contains oleylamine capped Au NPs@SiNWs /Br^- /Br_3^-/ C fabric. For AuNPs an absorption peak at 550 nm is observed which is attributed to Surface Plasmon Resonance. Although AuNPs are well known electrocatalytic materials but its deposition on SiNWs does not improve power conversion efficiency which is evident from the table 4.3.11. Similarly, a relative impedance spectrum for AuNPs@SiNWs and SeNPs@SiNWs based device is shown in figure 4.3.11(c). According to which the recombination resistance for AuNPs@SiNWs is 2.18 Ω and for SeNPs based device it is 1.69 Ω. But this lowering in recombination resistance is compensated by hole transporting property of SeNPs be cause of which efficiency is higher for SeNPs decorated SiNWs device.

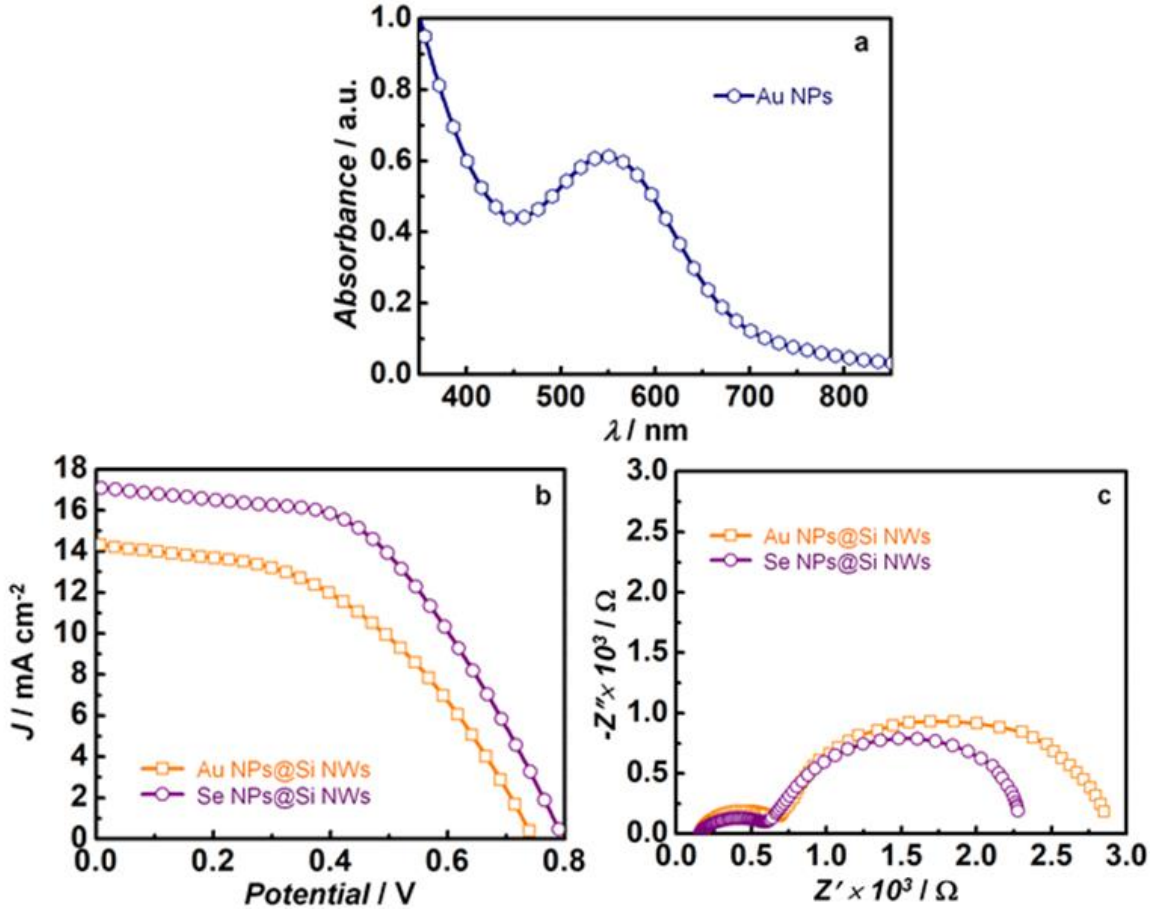

Figure 4.3.11: Absorption spectra of Au NPs. (b) J-V curves of the cells with Au NPs@Si NWs and Se NPs@Si NWs photoanodes under 100 mW cm^{-2} and (c) Nyquist plots of the same cells with photoanode-Br^-/Br_2-C-fabric configurations in dark, over a frequency range of 10^6 to 0.1 Hz at V_{OC}.

Table 4.3.11: Comparison between the solar cell parameters of Au NPs@Si NWs/Br^-/Br_3^-/C-fabric control cell, Se NPs@Si NWs photoanode and Si NWs based cell (active area 0.5 cm^2).

Photoanode	V_{OC} (mV)	J_{SC} (mA cm^{-2})	FF (%)	Efficiency (η %)
Si NWs	734	13.88	48.23	4.91
Se NPs@Si NWs	790	17.12	51.96	7.03
Au NPs@Si NWs	739	14.32	46.83	4.96

5. ALTERNATE HTL AND CE

In this work, other materials have been made to modify the photoanode, replace the electrolyte and counter electrode to improve the solar cell efficiency and device stability. Although the results are not so good but it provides deep insights on the device architecture and stability.

5.1 Photoanode

Hole transporting polymer like PEDOT is electrodeposited over SiNWs to check whether it can participate in hole transportation like SeNPs.[21] The result is given in the following table.

5.1.1 Synthesis of PEDOT/ SiNWs[21]

258 μL of 0.1(M) EDOT is dissolved in 20 mL acetonitrile solvent. To this solution 0.2 gm $LiClO_4$ is added to increase the conductivity of the solution. PEDOT is electrodeposited over SiNWs having Ag/AgCl as reference electrode and Pt as counter electrode under 1V.

Table 5.1: Solar cell parameters of PEDOT@SiNWs/Br^-/Br_2/C fabric cell under 1sun illumination.

Photoanode	V_{OC} (mV)	J_{SC} (mA cm^{-2})	FF (%)	Efficiency (η %)
PEDOT@SiNWs	580	1.2	19.6	0.13

5.2 Counter electrode

Attempts have been made to replace the non-transparent C fabric electrode with a transparent electrode like FTO so that a sandwich type of device can be made. To further increase electrical conductivity, a very thin film of electrochromic transition metal oxides like WO_3 and PEDOT are electrodeposited over transparent FTO. For similar reasons, CNT was also dropcast over SiNWs to check device performance.

5.2.1 Synthesis of WO_3/FTO[22]

In a 10 mL of hydrogen peroxide solution 1 gm of tungsten powder is added slowly. The solution is left for aging for couple of hours to complete the exothermic dissolution of the metal powder in H_2O_2. This pale yellow colored polyperoxotungstic acid is used as a precursor solution. FTO is used as working electrode and Ag/AgCl and Pt rod as reference electrode and counter electrode respectively. A fixed dc bias of -0.5 V is applied for 5 min and a deep blue colored film of WO_{3-x} formed over FTO.

Table 5.2 Solar cell parameters of SeNPs@SiNWs/Br^-/Br_2/CE cell under 1sun illumination with different CEs.

Counter electrode	V_{OC} (mV)	J_{SC} (mA cm^{-2})	FF (%)	Efficiency (η %)
WO_3@FTO	800	6.27	25.48	1.28
PEDOT@FTO	858	6.16	24.91	1.317
CNT@FTO	707	0.86	26.42	0.16

5.3 Electrolyte

The highly corrosive HBr/Br_2 redox electrolyte was replaced with less corrosive Br_2/ EMIBr and $Fe(CN)_6^{4-}$/ $Fe(CN)_6^{3-}$ redox electrolytes to improve the solar cell stability. Although the stability of the solar cell is improved, but the efficiency is very poor. This is due to the poor hole scavenging ability of the HTLs.

Table 5.3 Solar cell parameters of SiNWs/C fabric solar cell in different redox electrolyte under 1sun illumination.

Electrolyte	V_{OC} (mV)	J_{SC} (mA cm^{-2})	FF (%)	Efficiency (η %)
0.05M Br_2 in 8.6M EMIBr in PC	480	3.78	25.82	0.47
$Fe(CN)_6^{4-}$/ $Fe(CN)_6^{3-}$	320	0.29	35.46	0.03

6. CONCLUSION

In this work, a liquid junction Silicon nanowire solar cell was assembled. The photoanode was prepared by drop-casting t-Se nanoparticle over well etched SiNWs. The t-Se NPs being photoconductive facilitates radial junction hole transport and enhances power conversion efficiency compare to pristine SiNWs based solar cell. Also, the t-Se NPs being a light scattering material it causes electronic excitation in SiNWs causing electron-hole separation and favors charge transport. The counter electrode used was carbon fabric which is highly robust and conductive. The redox electrolyte used was mixture of 0.05M Br_2 in 8.6M HBr in an aqueous medium. Under illuminated condition, electronic excitation takes place in SiNWs and a hole is created in the valence band and that hole is captured by Se NPs which further goes on to react with reduced redox species i.e. Br^- and generates Br_3^-. This Br_3^- reacts with electrons in the counter electrode to produce Br^- and thereby completes the cycle and produces electricity. The PEC analysis data concur with the PCEs of the solar cells, thus recommending a well-tailored uniquely decorated Si NW array as a promising electrode for economical and scalable PV devices.

References

1. Bangall, D.M.; Boreland, M. *Energy Policy* **2008**, 36, 4390-4396.

2. Green, M.A. *Sol. Energy.* **2004**, 76, 3-8.

3. Law, M.; Greene, L.E.; Johnson, J.C.; Saykally, R.; Yang, P.D. *Nat. Mater.* **2005**, 4, 455.

4. Hu, L.; Chen, G. *Nano Lett.* **2007**, 7, 3249-3252.

5. Lewis, N.S. *Science* **2007**, 315, 798-801.

6. Peng, K.; Wang, X.; Lee, S.-T. *Appl. Phys. Lett.* **2008**, *92,* 163103.

7. Goodey, A.P.; Eichfeld, S.M.; Lew, K-K.; Redwing, J.M.; Mallouk, T.E. *J. Am. Chem. Soc.* **2007**, 129, 12344-12345.

8. Kamat, P.V.; Tvrdy, K.; Baker, D.R.; Radich, J.G. *Chem.Rev.* **2010**,110,6664-6668.

9. Shu, Q.; Wei, J.; Wang, K.; Zhu, H.; Li, Z.; Jia, Y.; Gui, X.; Guo, N.; Li, X.; Ma, C.; Wu, D. *Nano Lett.* **2009**,9, 4338-4342.

10. Peng, K. -Q.; Wang, X.; Wu, X. -L.; Lee, S.-T. *Nano Lett.* **2009**, *9*, 3704–3709.

11. Wang, X.; Peng, K. -Q.; Pan, X. -J.; Chen, X.; Yang, Y.; Li, L.; Meng, X. -M.; Zhang, W. -J.; Lee, S.-T. *Angew. Chem. Int. Ed.* **2011**, *50*, 9861–9865.

12. Shen, X.; Sun, B.; Yan, F.; Zhao, J.; Zhang, F.; Wang, S.; Zhu, X.; Lee, S. *ACS Nano* **2010**, *4*, 5869–5876.

13. Dalchiele, E. A.; Martín, F.; Leinen, D.; Marotti, R. E.; Ramos-Barrado, J. R. *J. Electrochem. Soc.* **2009**, *156*, 77–81.

14. Zhang, B.; Dai, W.; Ye, X.; Hou, W.; Xie, Y. *J. Phys. Chem. B* **2005**, *109*, 22830–22835.

15. Peng, B. K.; Lu, A.; Zhang, R.; Lee, S.-T. *Adv. Funct. Mater.* **2008**, *18*, 3026–3035.

16. Kolay, A.; Maity, D.; Ghosal, P.; Deepa, M. *J. Phys. Chem. C*. **2019**, 123(14), 8614-8622.

17. Ko, A. C.-T.; Hewko, M.; Sowa, M. G.; Dong, C. C. S.; Cleghorn, B.; Choo-Smith, L.-P. *Opt. Express* **2008**, *16*, 6274–6284.

18. Zhang, S.-Y.; Liu, Y.; Ma, X.; Chen, H.-Y. Rapid. *J. Phys. Chem. B*. **2006**, *110*, 9041–9047.

19. Sicha, M.; Studnicka, J.; Prosser, V.; Gruber, B. *Phys. Stat. Solidi* **1964**, *7*, 1045–1050.

20. Fuhs, W.; Stuke, J. *Phys. Stat. Solidi* **1968**, *27*, 171–184.

21. Liu, R.; Wang, J.; Sun, T.; Wang, M.; Wu, C.; Zou, C.; Song, T.; Zhang, X.; Lee, S-T.; Wang, Z-L.; Sun, B. *Nano Lett.* **2017**, 17, 4240-4247.

22. Kumar, P-N.; Kolay, A.; Kumar, S-K.; Patra, P-K.; Aphale, A-N.; Srivastava, A-K.; Deepa, M. ACS Appl. Mater. Interfaces. **2016**, 8(41), 27688-27700.